

December 22, 2022

Electroweak corrections to $g + g \rightarrow H_{l,h}$ and $H_{l,h} \rightarrow \gamma + \gamma$ in the Higgs-singlet extension of the Standard model

Christian Sturm^{a,1}, Benjamin Summ^{a,2} and Sandro Uccirati^{b,3}

^a *Universität Würzburg,
Institut für Theoretische Physik und Astrophysik,
Lehrstuhl für Theoretische Physik II,
Campus Hubland Nord,
Emil-Hilb-Weg 22,
D-97074 Würzburg,
Germany*

^b *Università di Torino e INFN,
10125 Torino,
Italy*

Abstract

We calculate the next-to-leading order electroweak corrections for Higgs-boson production in gluon fusion and the Higgs-boson decay into two photons or gluons in the real Higgs-singlet extension of the Standard model (HSESM). For the light Higgs-boson of the HSESM the electroweak corrections for these processes are of the same order of magnitude as in the Standard model. For the heavy Higgs-boson of the HSESM the electroweak corrections can become large depending on the considered scenario.

¹Christian.Sturm@physik.uni-wuerzburg.de

²Benjamin.Summ@physik.uni-wuerzburg.de

³uccirati@to.infn.it

1 Introduction

The discovery of a Higgs boson at the Large Hadron Collider (LHC) [1] was a tremendous success and the beginning of detailed studies of its properties. One important question is, whether the discovered Higgs boson is just the Standard model (SM) Higgs boson or whether it is part of a more general Higgs sector. One of the simplest extensions of the SM Higgs sector is the one where one adds an additional electroweak scalar singlet field S to the SM field content [2, 3].

In general one can distinguish two types of Higgs-Singlet Extensions of the SM (HSESM); the real singlet extension of the SM and the complex singlet extension of the SM. In the case of the real HSESM one has one additional physical Higgs boson H_h which we consider as heavy compared to the light observed Higgs boson H_l with mass $M_{H_l} \equiv M_h = 125.25$ GeV [4]. In the real HSESM one has only three new additional free parameters compared to the SM, which can be expressed in terms of the new heavy Higgs-boson mass M_{H_h} , the ratio of two vacuum expectation values, conventionally denoted by $\tan \beta$, and a mixing angle α . The complex HSESM can have in addition other two free parameters. For certain configurations of these parameters the HSESM can provide candidates for dark matter. In the following we will consider a real scalar Higgs singlet S which has a vacuum expectation value (vev) as well as a discrete Z_2 symmetry, $S \rightarrow -S$, so that terms which are odd in S do not appear in the potential. The HSESM is being scrutinized by the ATLAS and CMS collaborations [5, 6] by deriving bounds and constraints on its new parameters.

Next-to-leading order (NLO) electroweak (EW) corrections to light and heavy Higgs-boson production in Higgs strahlung and to Higgs-boson production in vector-boson fusion as well as the NLO results on the four-fermion (f) decays $H_{l,h} \rightarrow WW/ZZ \rightarrow 4f$ have been computed in Refs. [7, 8, 9]. Interference effects at the one-loop level for the W^+W^- and $t\bar{t}$ decay modes with fully leptonic WW decay have been studied in Ref. [10]. NLO electroweak corrections to the heavy-to-light Higgs-boson decay have been determined in Ref. [11]. The low energy behaviour of the HSESM has been studied in Ref. [12].

Theoretical and experimental constraints and their impact on the allowed parameter space as well as benchmark scenarios for searches for an additional Higgs singlet have been studied in Ref. [13, 14]. Several benchmark scenarios have been summarized in the report of the LHC Higgs Cross Section Working Group (HXS WG) [15].

Within this work we focus on the loop-induced Higgs-boson production and decay processes. In the SM the complete electroweak corrections to Higgs-boson production in gluon fusion and the Higgs-boson decay into two photons are known since long [16, 17, 18]. In the HSESM theory predictions for cross sections of Higgs-boson production via gluon fusion at higher order in perturbative QCD can be obtained from the SM results, whereas higher order electroweak corrections in this model are still unknown for this process. In this paper we calculate the effect of the NLO electroweak corrections on the production of a light and a heavy Higgs boson through gluon (g) fusion, $g + g \rightarrow H_{l,h}$, in the real HSESM. Likewise we calculate the NLO electroweak correction of the Higgs-boson decay into two photons (γ) in the real HSESM for the light and heavy Higgs boson, $H_{l,h} \rightarrow \gamma + \gamma$,

which are also still unknown. The few new parameters in the model under consideration will allow us then to provide even scans over a wide range of the new input parameters, rather than restricting ourselves to benchmark points only, which makes our results more generally applicable, if further parameter regions will be experimentally excluded. In addition we provide results for the benchmark points collected in Refs. [14, 15, 8], which we will outline in more detail later in this work.

Electroweak corrections to loop-induced Higgs-boson production and decay processes can become large. This has been seen, for example, in the calculation of the electroweak corrections to Higgs-boson production through gluon fusion and the Higgs-boson decay into two photons in a SM with a sequential fourth generation of heavy fermions [19, 20]. Similarly the calculation of the two-loop, electroweak corrections to the production of a light and a heavy neutral, scalar Higgs-boson through the gluon fusion process in the Two-Higgs-Doublet Model(2HDM) [21, 22] also showed that the corrections can be sizable. The knowledge of the electroweak corrections in the HSESM is thus important.

The outline of this paper is as follows. In Section 2 we define the HSESM and its new parameters. Section 3 contains the details of our calculations and checks which we have performed. In Section 4 we present our results and discuss them. Finally we close with our summary and conclusions in Section 5.

2 The Higgs-Singlet Extension of the Standard model

The scalar potential of the Higgs-Singlet Extensions of the SM (HSESM), which satisfies a Z_2 symmetry, $S \rightarrow -S$, is given by

$$V_{\text{HSESM}} = m_1^2 \Phi^\dagger \Phi + m_2^2 S^2 + \frac{\lambda_1}{2} (\Phi^\dagger \Phi)^2 + \frac{\lambda_2}{2} S^4 + \lambda_3 \Phi^\dagger \Phi S^2, \quad (1)$$

where we have adopted the conventions of Ref. [7] with the scalar doublet field Φ and the scalar singlet field S . The parameters m_1^2 , m_2^2 and λ_i ($i = 1, 2, 3$) of the potential are all real. For

$$\lambda_1 > 0, \quad \lambda_2 > 0 \quad \text{and} \quad \lambda_3^2 < \lambda_1 \lambda_2 \quad (2)$$

the potential has a global minimum with non-vanishing vacuum expectation values (vevs) of the scalar fields. The last inequality follows from the requirement that the Hessian matrix is positive definite at the extremum. The Hessian matrix is up to a global factor the mass (squared) matrix M_{ij}^2 from Eq. (5) below. It is real symmetric and thus orthogonal diagonalizable with real eigenvalues.

The Higgs doublet Φ and the Higgs singlet S are parameterized as

$$\Phi = \begin{pmatrix} \phi^+ \\ \frac{1}{\sqrt{2}}(v + \rho_1 + i\eta) \end{pmatrix}, \quad S = \frac{v_S + \rho_2}{\sqrt{2}}, \quad (3)$$

respectively, where η and ϕ^\pm are the would-be Goldstone-boson fields. Here, v and v_S are vacuum expectation values whose ratio is defined as $t_\beta \equiv \tan \beta = v_S/v$. The limit

$t_\beta \rightarrow 0$ corresponds to the limit of a vanishing vev $v_S \rightarrow 0$. After spontaneous symmetry breaking the real fields ρ_1 and ρ_2 mix to produce the mass eigenstates H_h and H_l through a orthogonal matrix

$$\begin{pmatrix} \rho_1 \\ \rho_2 \end{pmatrix} = \begin{pmatrix} \cos \alpha & -\sin \alpha \\ \sin \alpha & \cos \alpha \end{pmatrix} \begin{pmatrix} H_l \\ H_h \end{pmatrix}. \quad (4)$$

This rotation to the mass eigenstates diagonalizes the mass (squared) matrix

$$M_{ij}^2 = \left. \frac{\partial^2 V_{\text{HSESM}}}{\partial \rho_i \partial \rho_j} \right|_{\rho_{i,j}=0, \eta=0, \phi^\pm=0}, \quad (i, j = 1, 2), \quad (5)$$

which has eigenvalues $M_{H_l}^2$ and $M_{H_h}^2$ that satisfy $M_{H_l} < M_{H_h}$. The angle α is restricted to the interval $(-\pi/2, \pi/2]$. The real scalar fields satisfy the minimum conditions for the scalar potential

$$\langle \rho_i \rangle = 0, \quad (i = 1, 2). \quad (6)$$

Using these conditions and the rotation into the basis of mass eigenstates one can express the potential parameters through the physical input parameters, i.e. the masses of the light and heavy Higgs boson, M_{H_l} and M_{H_h} as well as the mixing angle α , the ratio of the vevs $\tan \beta$ and the vev v . The quartic couplings take the form

$$\lambda_1 = \frac{M_{H_l}^2}{v^2} \cos^2 \alpha + \frac{M_{H_h}^2}{v^2} \sin^2 \alpha, \quad (7)$$

$$\lambda_2 = \frac{M_{H_l}^2}{v^2 \tan^2 \beta} \sin^2 \alpha + \frac{M_{H_h}^2}{v^2 \tan^2 \beta} \cos^2 \alpha, \quad (8)$$

$$\lambda_3 = \frac{M_{H_l}^2 - M_{H_h}^2}{2v^2 \tan \beta} \sin(2\alpha). \quad (9)$$

Instead of the ratio of the vevs $\tan \beta$ one can also use λ_3 as an input parameter by expressing $\tan \beta$ in terms of λ_3 with the help of Eq. (9). As per usual the vev v is fixed through its relation to the W -boson mass M_W and the weak isospin gauge coupling g , which is the same in the HSESM as in the SM

$$M_W = \frac{1}{2} g v. \quad (10)$$

As can be seen from Eq. (8) the coupling λ_2 is quadratically enhanced(suppressed) for small(large) values of $\tan \beta$. The coupling λ_3 is the only coupling of the Higgs sector that depends on the sign of the mixing angle α . If the mixing angle α is negative(positive), the coupling λ_3 of Eq. (9) is always positive(negative), since $M_{H_l} < M_{H_h}$ and $\tan \beta > 0$. The inequalities in (2) are equivalent to requiring that the quadratic physical Higgs-boson masses are positive. Inserting Eqs. (7)-(8) into the expressions for $m_{1,2}$ derived from the extremal condition of the potential one finds

$$m_1^2 = -\frac{M_{H_l}^2 \cos^2 \alpha + M_{H_h}^2 \sin^2 \alpha}{2} + \frac{M_{H_h}^2 - M_{H_l}^2}{4} \sin(2\alpha) \tan \beta, \quad (11)$$

$$m_2^2 = -\frac{M_{H_h}^2 \cos^2 \alpha + M_{H_1}^2 \sin^2 \alpha}{2} + \frac{M_{H_h}^2 - M_{H_1}^2}{4} \frac{\sin(2\alpha)}{\tan \beta}. \quad (12)$$

We have assumed to have two non-vanishing vevs, so that one can expect that at least one of the two parameter m_1^2 and m_2^2 has to be negative⁴, however the other can also be positive.

Note that the doublet Φ couples to gauge bosons and fermions in exactly the same way as in the SM and the only effect of the Higgs singlet is that there is Higgs mixing. Therefore the tree-level couplings of H_1 and H_h to gauge bosons and fermions are the same as those of the SM Higgs boson, but scaled by the respective trigonometric function of the mixing angle α . We also note that t_β only appears in purely scalar tree-level vertices, which are polynomials of degree at most two in $1/t_\beta$.

3 Calculation

3.1 Generalities

The leading-order (LO) partial decay width Γ of a Higgs boson H of the HSESM decaying into two photons (γ) is given by

$$\Gamma_{\text{HSESM}}^{\text{LO}}(H \rightarrow \gamma + \gamma) = \frac{G_F M_H^3 \alpha_{\text{em}}^2}{32\sqrt{2}\pi^3} c_H^2 |A_{\gamma\gamma}^{\text{LO}}|^2, \quad (13)$$

where H stands here and in the following for either the light or the heavy Higgs boson, H_1 or H_h ; G_F is the Fermi-coupling constant and α_{em} the fine-structure constant. The coefficient c_H is given by

$$c_{H_1} = \cos(\alpha), \quad c_{H_h} = -\sin(\alpha), \quad (14)$$

where the SM limit corresponds to $\sin \alpha \rightarrow 0$, $\cos \alpha \rightarrow 1$ and is at LO independent of $\tan \beta$. Considering higher order electroweak corrections the new Higgs sector decouples when sending in addition $\tan \beta \rightarrow \infty$. The dimensionless amplitude $A_{\gamma\gamma}^{\text{LO}}$ can be decomposed into a fermionic (fer) and bosonic (bos) contribution $A_{\gamma\gamma}^{\text{LO}} = A_{\text{fer}} + A_{\text{bos}}$. The fermionic contribution can again be subdivided into a part which arises from leptons A_l and one which arises from quarks A_q , i.e. $A_{\text{fer}} = \sum_l Q_l^2 A_l + N_c \sum_q Q_q^2 A_q$, where Q_l and Q_q are the electric charges of the fermions in units of the elementary charge and N_c is the number of colours. The sum runs over all charged leptons l and quarks q . We only consider the top quark as massive and all other fermions as massless, so that only the term containing A_{top}

⁴If we would assume that m_1^2 and m_2^2 are both positive and use λ_3 from Eq. (9), this would lead to

$$-\frac{(M_{H_h}^2 - M_{H_1}^2)^2 \sin^2(2\alpha)}{4v^2(M_{H_1}^2 \cos^2 \alpha + M_{H_h}^2 \sin^2 \alpha)} < \lambda_3 < -\frac{M_{H_h}^2 \cos^2 \alpha + M_{H_1}^2 \sin^2 \alpha}{v^2}.$$

Multiplying this inequality by the positive factor $M_{H_1}^2 \cos^2 \alpha + M_{H_h}^2 \sin^2 \alpha$ one can see that the upper bound of λ_3 is smaller than the lower bound, leading to a contradiction.

will contribute to the dimensionless fermionic amplitude A_{fer} . Under these assumptions the dimensionless fermionic and bosonic amplitudes read

$$A_{\text{bos}}(\tau_W) = -1 - \frac{3}{2\tau_W} \left[1 + \left(2 - \frac{1}{\tau_W} \right) f(\tau_W) \right], \quad (15)$$

$$A_{\text{top}}(\tau_t) = \frac{1}{\tau_t} \left[1 + \left(1 - \frac{1}{\tau_t} \right) f(\tau_t) \right], \quad (16)$$

with $\tau_p = M_H^2/(4M_p^2)$ ($p \in \{t, W\}$). The function $f(\tau)$ is given by

$$f(\tau_p) = \begin{cases} \arcsin^2 \sqrt{\tau_p}, & \text{if } \tau_p \leq 1, \\ -\frac{1}{4} \left[\ln \left(\frac{1+\sqrt{1-1/\tau_p}}{1-\sqrt{1-1/\tau_p}} \right) - i\pi \right]^2, & \text{if } \tau_p > 1. \end{cases} \quad (17)$$

The real and imaginary parts of the purely bosonic and fermionic dimensionless amplitudes of Eqs. (15) and (16) have opposite signs in the whole Higgs-boson mass range, see Fig. 1. The imaginary parts are zero below the WW and $t\bar{t}$ threshold, respectively, up to tiny contributions from the finite widths in the complex mass scheme.

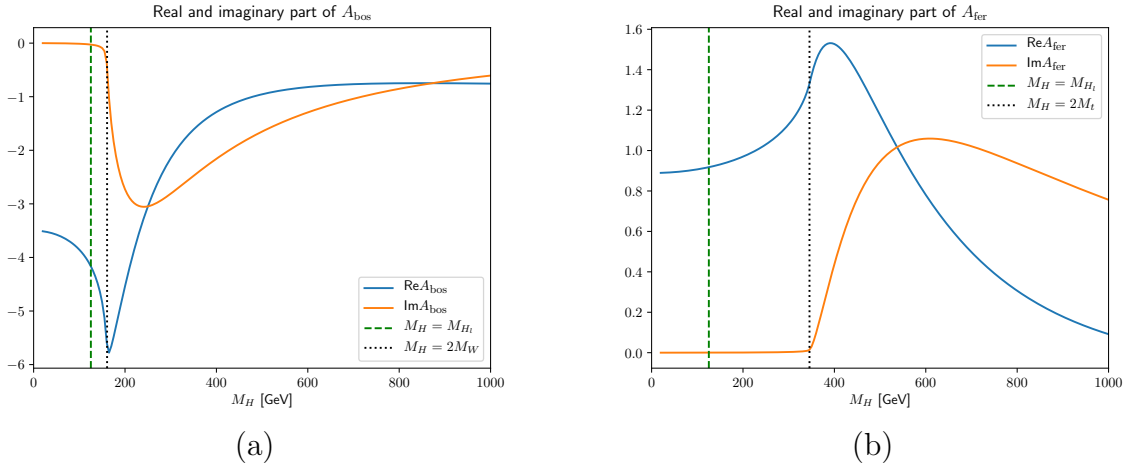


Figure 1: Real (a) and imaginary (b) part of the bosonic and fermionic contribution to $A_{\gamma\gamma}^{\text{LO}}$, respectively. The vertical dashed line denotes the location of the SM Higgs-boson $M_H = M_{H_l} = 125.25$ GeV. The vertical dotted lines indicate the location of the WW - and $t\bar{t}$ -thresholds. The dimensionless amplitudes are evaluated with complex masses as described in Section 3.2.

In particular for Higgs-boson masses above about $M_H \approx 500$ GeV one can observe strong cancellations between the dimensionless bosonic and fermionic amplitude, so that the real and imaginary parts of the total dimensionless amplitude have modulus smaller than one, see Fig. 2(a). Therefore the modulus squared of the total dimensionless amplitude is very small in this mass range, see Fig. 2(b). Such cancellations, which lead to a small dimensionless LO amplitude, can cause the relative NLO corrections to be huge, although

the absolute size of the NLO corrections is reasonable. We will observe exactly this situation in Section 4.2. A similar observation was made in studying a sequential fourth generation of heavy fermions [20]. In addition to these cancellations there is a minimum

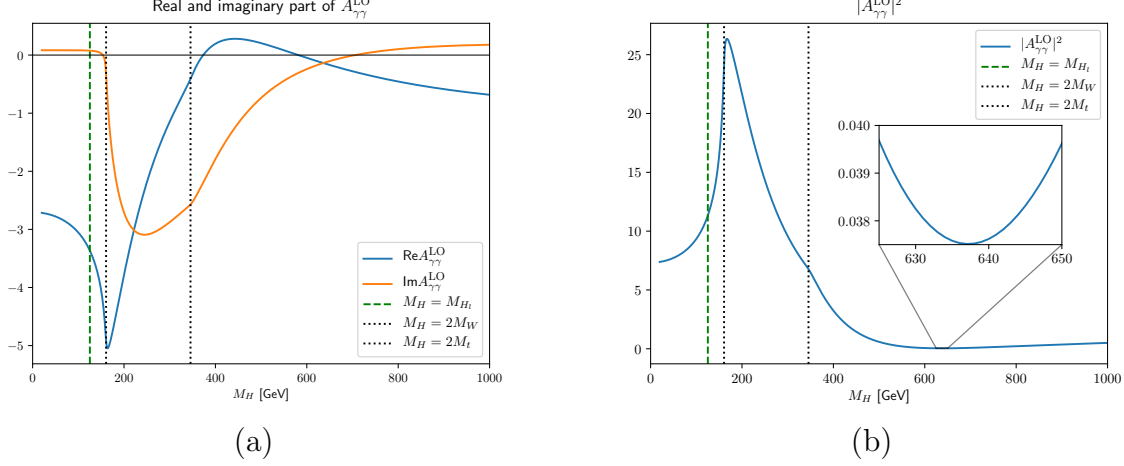


Figure 2: The real and imaginary part of the full dimensionless amplitude $A_{\gamma\gamma}^{\text{LO}}$ (left) and its squared modulus (right). The vertical dashed line denotes the location of the SM Higgs-boson $M_H = M_{H_t} = 125.25$ GeV. The vertical dotted lines indicate the location of the WW - and $t\bar{t}$ -thresholds. The dimensionless amplitudes are evaluated with complex masses as described in Section 3.2.

of the modulus squared of the dimensionless amplitude around $M_H \sim 630 - 640$ GeV, see inset of Fig. 2(b), which is even more enhanced for the decay width of a heavy Higgs-boson, as can be seen in Fig. 3(a). The reason for the enhancement is the overall factor of M_H^3 in Eq. (13) which causes the partial decay width to grow for large values of the heavy Higgs-boson mass M_{H_h} .

The leading-order cross section for the production of a Higgs boson H of the HSESM through gluon fusion is given by

$$\begin{aligned} \sigma_{\text{HSESM}}^{\text{LO}}(g + g \rightarrow H) &= \frac{G_F M_H^2 \alpha_s^2}{128 \sqrt{2} \pi} c_H^2 |A_{gg}^{\text{LO}}|^2 \delta(s - M_H^2) \\ &= \hat{\sigma}^{\text{LO}} M_H^2 \delta(s - M_H^2), \end{aligned} \quad (18)$$

with the strong coupling constant α_s and the dimensionless amplitude $A_{gg}^{\text{LO}} = A_{\text{top}}(\tau_t)$ from Eq. (16). We consider again only the top-quark as a massive fermion and all other quarks as massless. Likewise the partial decay width for the Higgs-boson decay into two gluons is given by

$$\Gamma_{\text{HSESM}}^{\text{LO}}(H \rightarrow g + g) = \frac{G_F M_H^3 \alpha_s^2}{16 \sqrt{2} \pi^3} c_H^2 |A_{gg}^{\text{LO}}|^2. \quad (19)$$

For the inclusion of the NLO electroweak corrections we write the dimensionless amplitudes as

$$A_z = A_z^{(1)} + g_W^2 A_z^{(2)} + \mathcal{O}(g_W^4), \quad g_W^2 = \frac{G_F M_W^2}{8 \sqrt{2} \pi^2}, \quad (20)$$

where z denotes the process, either $z = \gamma\gamma$ or $z = gg$. The one-loop LO dimensionless amplitude is given by $A_z^{(1)} \equiv A_z^{\text{LO}}$ and similarly $A_z^{(2)}$ is the two-loop dimensionless amplitude containing the electroweak corrections. The NLO electroweak percentage corrections δ_{EW} are then given by

$$|A_z|^2 = |A_z^{(1)}|^2 (1 + \delta_{\text{EW}}), \quad \text{with} \quad \delta_{\text{EW}} = \frac{2 \text{Re}[g_W^2 A_z^{(2)} A_z^{(1)\dagger}]}{|A_z^{(1)}|^2}. \quad (21)$$

Let us remark that in the determination of the electroweak percentage corrections of Eq. (21) the overall factors of Eq. (13) and (18) cancel for both processes; in particular the overall Higgs-boson mass dependence drops out. Hence δ_{EW} as defined in Eq. (21) describes the electroweak percentage corrections of the partial decay width and partonic cross section.

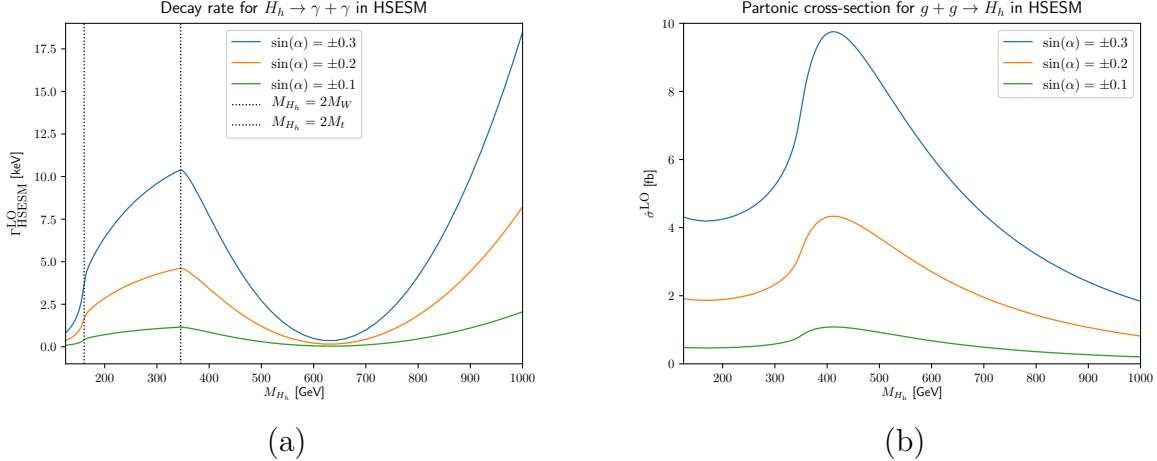


Figure 3: The LO partial decay width for $H_h \rightarrow \gamma + \gamma$ (a) and the LO partonic cross-section for $g + g \rightarrow H_h$ (b).

In Fig. 3 we show the LO partial decay width of Eq. (13) for the process $H_h \rightarrow \gamma + \gamma$ as well as the partonic LO cross section $\hat{\sigma}^{\text{LO}}$ of Eq. (18) for the process $g + g \rightarrow H_h$ as a function of the heavy Higgs-boson mass for three different values of $\sin \alpha$ evaluated numerically with the input parameters of Eqs. (28). For the process $g + g \rightarrow H_h$ we use a running strong coupling constant α_s [23]. In Fig. 3(a) one can see a clear maximum at $M_{H_h} = 2M_t$ corresponding to the $t\bar{t}$ -threshold of the top-triangle and a kink at $M_{H_h} = 2M_W$, which corresponds to the WW -threshold present in the bosonic contribution of the process $H_h \rightarrow \gamma + \gamma$.

3.2 Outline of the calculation

Feynrules [24] was employed to generate all Feynman rules that are independent of gauge parameters, while the gauge-fixing vertices were implemented separately in the t'Hooft-Feynman gauge. All diagrams were generated using QGRAF [25] and the resulting expressions were manipulated using the in-house code QGS, which is based on FORM [26].

The program QGS is an extension of GraphShot(GS), already used for these same processes in the SM [16, 17]. QGS has been extended to work within the 2HDM [22] and now the HSESM. The code, after performing the standard operations connected to the Dirac algebra with an anticommuting γ_5 (no anomalous diagrams are present for the processes under consideration), identifies the Lorentz structures of the amplitude by using projectors. This allows for a fast computation of the amplitude by only considering those Lorentz structures which enter in the squared amplitude of the physical process at the end of the calculation. In a next step the obtained expressions are simplified by removing reducible scalar products and using symmetries. This allows to reduce the amplitude to a combination of a small set of tensor integrals contracted with external momenta, which can be considered as the master integrals of the process under consideration. The UV-divergent part of these integrals is then extracted and canceled analytically against the analogous part of the counterterms, which do not depend on the specific renormalization scheme adopted. The inclusion of the finite part of the counterterms, which we call finite renormalizations, will be discussed in the next Section 3.3. The obtained UV-finite amplitude still contains divergent integrals due to collinear singularities related to massless fermions. Since the electroweak corrections for both processes can not be divergent (there is no real emission which could compensate such singularities), we extract the divergent behaviour of each integral as logarithms in a small fictitious fermion mass and verify their cancellation analytically. The remaining loop integrals are then written in Feynman-parametric spaces in a form suited for numerical evaluation, following the techniques described in Refs. [27, 18]. The integrands of the obtained integrals are then collected in a Fortran library and the whole amplitude is evaluated numerically with the desired numerical accuracy using an in-house integrator based on the Korobov-Conroy number theoretic methods [28]. Here we need to evaluate integrals up to dimension five numerically.

3.3 Renormalization

For the renormalization procedure of the SM parameters of the two processes $g + g \rightarrow H_{l,h}$ and $H_{l,h} \rightarrow \gamma + \gamma$ we follow closely the SM case of Refs. [16, 18]. For the renormalization of the W - and Z -boson masses as well as for the top-quark mass we use the complex mass scheme [29], where all parameters of the theory which depend on M_W , M_Z and M_t become complex.

Concentrating on the new parameters of the HSESM discussed in Section 2, we see that there are the ratio of the vevs $\tan\beta$ and the mixing angle α which are not present in the SM. For a complete renormalization of the HSESM both of these parameters have to be renormalized. However, for the processes under consideration in this work, it is sufficient to renormalize the mixing angle α since $\tan\beta$ does not appear at LO.

A $\overline{\text{MS}}$ renormalization of these two parameters of the HSESM requires a proper treatment of the Higgs tadpoles in order to obtain gauge-independent results for physical observables. The Fleischer-Jegerlehner(FJ)-tadpole scheme was introduced for a consistent treatment of the Higgs-tadpoles in the SM [30]. The FJ tadpole scheme in the SM

is equivalent to the β_t scheme of Ref. [31]. The FJ tadpole scheme has been extended for a general Higgs sector in Ref. [21], which we apply here for the HSESM. In Refs. [32] a new scheme for tadpole renormalization, dubbed gauge-invariant vacuum expectation value scheme, was introduced being perturbatively stable. Its implementation is beyond the scope of the current work.

A $\overline{\text{MS}}$ renormalization of mixing angles can lead to unnatural large corrections and can suffer from a large scale dependence. Within this work we focus on the renormalization schemes for the mixing angle α in the HSESM which were proposed in Ref. [9]. In particular we discuss three schemes dubbed ZZ scheme, $\overline{\Psi\Psi}$ scheme and OS scheme in the following.

First, the amplitudes for the decays of the two Higgs-bosons of the HSESM into two Z bosons were used in Ref. [9] in order to define a physical renormalization scheme. At LO they read $\mathcal{M}_{H \rightarrow Z+Z}^{(0)} = -c_H M_W e / (s_W c_W^2) (\varepsilon_1^* \varepsilon_2^*)$, ($H = H_l$ or H_h), where e is the elementary charge, $s_W(c_W)$ is the sine(cosine) of the weak mixing angle, ε_i ($i = 1, 2$) are the two polarization vectors of the external Z bosons and c_H is defined in Eq. (14). After all other parameters have been renormalized the renormalization condition for the mixing angle α requires that the ratio of the two amplitudes

$$\frac{\mathcal{M}_{H_h \rightarrow Z+Z}}{\mathcal{M}_{H_l \rightarrow Z+Z}} \stackrel{!}{=} -\frac{\sin(\alpha)}{\cos(\alpha)} \quad (22)$$

is equal to its LO value [9], where we have adapted the condition to the definition of the mixing angle used in our work. Denoting bare quantities with a subscript B the bare mixing angle α_B is related to the renormalized one through the counterterm $\delta\alpha$ as $\alpha_B = \alpha + \delta\alpha$. Similarly, the bare and renormalized mass eigenstates of the heavy and light Higgs boson fields of Eq. (4) are related by the renormalization constants δZ_{ij} ($i, j \in \{H_l, H_h\}$) through

$$\begin{pmatrix} H_{h,B} \\ H_{l,B} \end{pmatrix} = \begin{pmatrix} 1 + \frac{1}{2}\delta Z_{H_h H_h} & \frac{1}{2}\delta Z_{H_h H_l} \\ \frac{1}{2}\delta Z_{H_l H_h} & 1 + \frac{1}{2}\delta Z_{H_l H_l} \end{pmatrix} \begin{pmatrix} H_h \\ H_l \end{pmatrix}. \quad (23)$$

Using the renormalization condition of Eq. (22) the counterterm of the mixing angle can be written as [9]

$$\delta\alpha = c_\alpha s_\alpha (\delta_{H_l ZZ} - \delta_{H_h ZZ}) + \frac{1}{2} c_\alpha s_\alpha (\delta Z_{H_l H_l} - \delta Z_{H_h H_h}) - \frac{1}{2} (\delta Z_{H_h H_l} s_\alpha^2 - \delta Z_{H_l H_h} c_\alpha^2), \quad (24)$$

where $c_\alpha = \cos(\alpha)$, $s_\alpha = \sin(\alpha)$ and $\delta_{H_i ZZ}$ ($i \in \{l, h\}$) are the unrenormalized relative one-loop corrections to the two decays. In practical applications a choice of the polarization vectors has to be made. If one considers the amplitudes of these two decays at LO without the external polarization vectors ε_i , their Lorentz structure consists only of the metric tensor. Considering higher order corrections additional tensor structures arise, which depend on the external momenta. We have studied several physical renormalization schemes already in Ref. [22] in the context of the 2HDM, where also the Higgs boson decay into two Z bosons was considered in a renormalization condition. There we required as

renormalization condition that the coefficient of the metric tensor in the above tensor decomposition of the amplitude is equal to its LO value. Similarly as in the 2HDM, we choose the polarization vectors of the external Z bosons here in the HSESM in such a way that all additional tensors vanish and only the form factor of the metric tensor survives. We will call this scheme ZZ scheme in the following.

A second renormalization scheme was defined in Ref. [9] by adding a fermion singlet field Ψ to the field content of the HSESM and coupling it to the singlet scalar through a Yukawa coupling which is sent to zero in order to recover the original theory. As renormalization condition for the mixing angle α one considers here again the decays of the light and heavy Higgs bosons, this time into a pair of the new singlet fields Ψ , and again requires that the ratio of the two amplitudes is equal to its LO value in the limit of vanishing coupling:

$$\frac{\mathcal{M}_{H_h \rightarrow \Psi + \bar{\Psi}}}{\mathcal{M}_{H_l \rightarrow \Psi + \bar{\Psi}}} \stackrel{!}{=} \frac{\mathcal{M}_{H_h \rightarrow \Psi + \bar{\Psi}}^{(0)}}{\mathcal{M}_{H_l \rightarrow \Psi + \bar{\Psi}}^{(0)}}. \quad (25)$$

From this renormalization condition, the counterterm of the mixing angle α can be calculated to be [9]

$$\delta\alpha = -\frac{1}{2}c_\alpha s_\alpha (\delta Z_{H_l H_l} - \delta Z_{H_h H_h}) - \frac{1}{2}(\delta Z_{H_h H_l} c_\alpha^2 - \delta Z_{H_l H_h} s_\alpha^2). \quad (26)$$

This scheme will be denoted in the following as $\bar{\Psi}\Psi$ scheme. We note that, as opposed to the ZZ scheme, the counterterm of the $\bar{\Psi}\Psi$ scheme does not depend on the unrenormalized one-loop corrections of the defining decays. This is due to the fact that these vanish in the limit of vanishing Yukawa coupling.

The explicit counterterms for the mixing angle α for the above two schemes were already given in Ref. [9], which we adapted to our conventions. A drawback of the ZZ and $\bar{\Psi}\Psi$ schemes is that they introduce artificial thresholds for the processes $g + g \rightarrow H_l$ and $H_l \rightarrow \gamma + \gamma$ when the heavy Higgs boson mass M_{H_h} is equal to twice the light Higgs boson mass M_{H_l} , as we will see explicitly in Section 4. These thresholds originate from the wave function factor of the heavy Higgs boson, which enters the counterterm of the mixing angle through the decay amplitude of the heavy Higgs boson. Interestingly, the threshold singularities induced in this way, have opposite signs in the two schemes as can be seen from Eqs. (24) and (26). This is due to the fact that in the ZZ scheme the couplings are induced by ρ_1 , which couples to gauge bosons, whereas in the $\bar{\Psi}\Psi$ scheme the couplings are induced by ρ_2 .

In the third and last scheme which we will consider in this paper the counterterm $\delta\alpha$ of the mixing angle α is fixed through the non-diagonal field renormalization constants of the light and heavy Higgs boson, avoiding the introduction of a threshold at $M_{H_h} = 2M_{H_l}$ in processes with a light external Higgs boson. The counterterm $\delta\alpha$ in this scheme is simply given by

$$\delta\alpha = \frac{\delta Z_{H_h H_l} - \delta Z_{H_l H_h}}{4}. \quad (27)$$

This renormalization condition has been introduced for the 2HDM and the HSESM [33, 9]. The non-diagonal field renormalization constants can be expressed in terms of the

non-diagonal, on-shell Higgs-boson mixing self-energies in the background-field method. We use here the conventional formalism which requires extra terms which are given in appendix B of Ref. [9]. We will label this scheme in the following as on-shell(OS) scheme.

3.4 Checks

Several checks were performed to validate the set-up and the correctness of the computation. The UV- and tadpole renormalization procedures were validated by checking analytically that the amplitudes are UV-finite after renormalization. We implemented the FJ tadpole scheme for the HSESM and verified that the physical counterterms are independent of gauge parameters in a general R_ξ gauge. The finite renormalization was validated by checking that the dependence on the renormalization scale μ cancels in the three renormalization schemes described earlier in this section. The Feynman rules were checked by comparing the amplitudes for the processes $H_l \rightarrow Z + Z$, $H_h \rightarrow Z + Z$ and $H_h \rightarrow H_l + H_l$ as well as for $g + g \rightarrow H_l$, $g + g \rightarrow H_h$, $H_l \rightarrow \gamma + \gamma$ and $H_h \rightarrow \gamma + \gamma$ with Recola [7, 34] at LO and at NLO for the non loop-induced processes. The processes $H_l \rightarrow Z + Z$ and $H_h \rightarrow Z + Z$ were compared in the $\overline{\text{MS}}$, OS and $\overline{\Psi\Psi}$ schemes, whereas the process $H_h \rightarrow H_l + H_l$ was checked in the $\overline{\text{MS}}$ scheme only, since it requires additional renormalization of the parameter $\tan\beta$ in the other schemes. We checked that the amplitudes for the processes $H_l \rightarrow Z + Z$ and $H_h \rightarrow Z + Z$ fulfill indeed the renormalization condition of Eq. (22) at NLO in the ZZ scheme. The appropriate IR behaviour of the amplitudes of the processes $g + g \rightarrow H_l$, $H_l \rightarrow \gamma + \gamma$, $g + g \rightarrow H_h$ and $H_h \rightarrow \gamma + \gamma$ was guaranteed by checking that the collinear singularities cancel as already described in Section 3.2. Furthermore, for all four processes it was checked that the Ward identity is satisfied. For the processes $g + g \rightarrow H_l$ as well as $H_l \rightarrow \gamma + \gamma$ the corresponding amplitudes in the HSESM were found to agree analytically with the corresponding SM amplitudes in the SM limit of the HSESM. We checked our numerical integration by scaling all integrals through the introduction of a scaling parameter s for all four processes. The scaling parameter s cancels in the total amplitude. The value of the part of the amplitude which contains integrals of the same integration dimension, however, depends on the specific choice of s . These differences cancel in the sum of all integration dimensions. We checked that the numerical value of the total amplitude is not affected by varying the value of s .

4 Results and discussion

In this section, we present the numerical results of phenomenologically interesting scenarios for light and heavy Higgs-boson production in gluon fusion and for the Higgs-boson decays into two photons. First, we consider the benchmark points (BPs) of Tab. 1. The BPs are taken from the LHC Higgs cross section working group report [15] and were proposed originally in Ref. [14]. We have adapted the input parameters of the BPs in Tab. 1 to our conventions of Section 2, i.e. in Ref. [14] the mixing angle α has opposite sign and $\tan\beta$ is given by the reciprocal value compared to Tab. 1.

BP	M_{H_h} [GeV]	$\sin(\alpha)$	$1/\tan(\beta)$
BHM200 \mp	200	∓ 0.29	1.19
BHM300 \mp	300	∓ 0.31	0.79
BHM400a \mp	400	∓ 0.26	0.58
BHM400b	400	+0.26	0.59
BHM500a \mp	500	∓ 0.24	0.46
BHM500b	500	+0.24	0.47
BHM600 \mp	600	∓ 0.22	0.38
BHM700a \mp	700	∓ 0.21	0.31
BHM700b	700	+0.21	0.32
BHM800a \mp	800	∓ 0.20	0.25
BHM800b	800	+0.20	0.27

Table 1: The benchmark points (BP) of Refs. [15, 14] are shown in our conventions. The mass of the heavy Higgs boson is encoded in the BP's name. The BPs which have the same heavy Higgs-boson mass, but the name differs by the suffix a or b have the same (positive) value of $\sin \alpha$ and are distinguished by a tiny difference in the value of $\tan \beta$.

Furthermore we show various plots which describe the impact of the electroweak corrections in terms of the mass of the heavy Higgs boson M_{H_h} for different values of $\sin \alpha$ and $\tan \beta$ in the OS scheme. First results for the renormalization of the mixing angle α in the ZZ -scheme were presented in Ref. [35]. Finally plots with the comparison of the three renormalization schemes for the mixing angle α are shown in dependence of the heavy Higgs-boson mass M_{H_h} , for specific values of $\sin \alpha$ and $\tan \beta$.

For the numerical evaluation we use the following input parameters from the PDG [4] for the particle masses and their total decay widths:

$$\begin{aligned}
M_t &= 172.76 \text{ GeV}, & M_Z &= 91.1876 \text{ GeV}, & M_W &= 80.379 \text{ GeV}, \\
\Gamma_t &= 1.42 \text{ GeV}, & \Gamma_Z &= 2.4952 \text{ GeV}, & \Gamma_W &= 2.085 \text{ GeV}, \\
M_{H_1} &= 125.25 \text{ GeV}, & \Gamma_{H_1} &= 0.0032 \text{ GeV}, & G_F &= 1.1663787 \cdot 10^{-5} \text{ GeV}^{-2}, \\
\alpha_s(M_Z) &= 0.1179, & \alpha_{\text{em}} &= 1/137.035999084.
\end{aligned} \tag{28}$$

We use the complex mass scheme [29] for the renormalization of the W - and Z -boson masses as well as for the top quark mass. For the two processes which have the heavy Higgs boson as an external particle, i.e. for heavy Higgs-boson production in gluon fusion and for the heavy Higgs-boson decay into two photons, the light Higgs boson appears only as an internal particle and is thus also renormalized in the complex mass scheme.

4.1 Higgs-boson production in gluon fusion in the HSESM

Choosing as reference renormalization scheme for the mixing angle α the OS scheme as defined in Section 3.3, we show in Fig. 4 the dependence of the electroweak percentage

corrections δ_{EW} defined in Eq. (21) on M_{H_h} for the production of the light Higgs boson at 6 values of $\sin \alpha$ for each plot. The values of $\sin \alpha$ are chosen to cover the allowed region of Ref. [6]. The three plots of Fig. 4 are for the three values of $\tan \beta = 1, 5$ and 10.

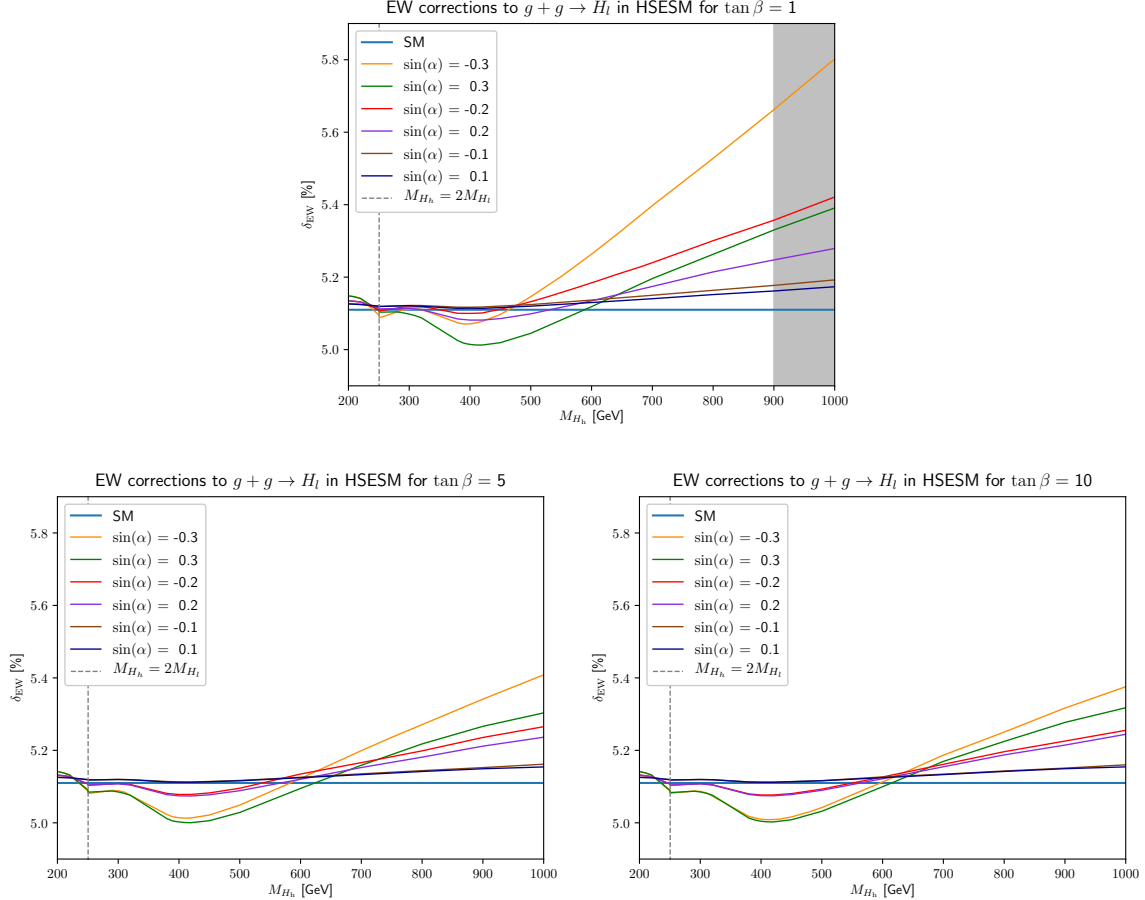


Figure 4: Relative NLO electroweak percentage corrections δ_{EW} in the OS scheme to the LO cross section of the process $g + g \rightarrow H_l$ in the HSES for $\tan \beta = 1, 5, 10$ with varying values of $\sin \alpha$. The SM limit is shown in blue.

The grey shaded area in the plot for $\tan \beta = 1$ indicates the onset of the non-perturbative regime, where at least one of the parameters $\frac{\lambda_i}{4\pi}$ ($i = 1, 2$ or 3) of Eq. (1) becomes larger than one. This only happens for small values of $\tan \beta$, since the latter appears in the denominator of Eqs. (8) and (9). The vertical dashed line indicates the location where the heavy Higgs-boson mass is twice the light Higgs-boson mass. All three plots of Fig. 4 show the same numerical range for the percentage correction and the heavy Higgs-boson mass in order to allow for a better comparison of the results for the three different values of $\tan \beta$. The electroweak corrections are very close to the ones in the SM (blue line), in the range of 5.0% – 5.8%, showing the largest deviations at high values of M_{H_h} , small values of $\tan \beta$ and large absolute values of $\sin \alpha$. The behaviour of δ_{EW} shows a small minimum around $M_{H_h} \approx 400$ GeV and grows almost linearly afterwards. For $\tan \beta = 1$ the

corrections are a little more enhanced than at $\tan \beta = 5$ and remain basically unchanged at larger values of $\tan \beta$. An interesting feature which we derive from the plots is the negligible dependence of the electroweak corrections on the sign of $\sin \alpha$ for large values of $\tan \beta$, revealing that the odd contributions in $\sin \alpha$ are $\tan \beta$ -suppressed. This can be seen best in the last plot of Fig. 4 (for $\tan \beta = 10$) where the lines for $\pm \sin \alpha$ approach each other and almost coincide. This feature can also be verified by inspecting the analytical expressions for the corrections.

For the BPs of Tab. 1 we show the electroweak percentage corrections in Tab. 2 for the process $g + g \rightarrow H_1$. The mixing angle α has been renormalized in the OS scheme. All BPs are very close to the SM result. For high values of the heavy Higgs boson mass (larger than 600 GeV) one can see a small increase of the percentage correction compared to the SM result. Considering BPs with a heavy Higgs-boson mass close to the minimum of Fig. 4 one can also see here a small decrease of the percentage correction.

BP	δ_{EW}	BP	δ_{EW}	BP	δ_{EW}
BHM200–	5.2	BHM400b	5.0	BHM700a–	5.2
BHM200+	5.1	BHM500a–	5.1	BHM700a+	5.2
BHM300–	5.1	BHM500a+	5.1	BHM700b	5.2
BHM300+	5.1	BHM500b	5.1	BHM800a–	5.2
BHM400a–	5.1	BHM600–	5.1	BHM800a+	5.2
BHM400a+	5.0	BHM600+	5.1	BHM800b	5.2

Table 2: The electroweak percentage corrections δ_{EW} [%] in the OS scheme are shown for the benchmark points of Tab. 1.

The electroweak percentage corrections which are provided in Fig. 4 and Tab. 2 also apply to the partial decay width of the process $H_1 \rightarrow g + g$ due to Eq. (19).

The same plots for the production of the heavy Higgs boson are shown in Fig. 5, which features larger (negative) electroweak percentage corrections compared to the production of the light Higgs boson. The axis of ordinates shows again the electroweak percentage correction δ_{EW} as a function of the heavy Higgs-boson mass M_{H_h} on the abscissa. Both axes show the same range of values for all three plots. Starting from around -3% for $M_{H_h} \approx 200$ GeV, the electroweak percentages corrections δ_{EW} increase to a maximum close to $\delta_{\text{EW}} \approx 0\%$ around $M_{H_h} \approx 350$ GeV and decrease then almost linearly to reach $\delta_{\text{EW}} \approx -15\%$ for $M_{H_h} \approx 1000$ GeV (and $\tan \beta = 1$). We see again a comparable behaviour for $\tan \beta = 5$ and $\tan \beta = 10$, while the corrections are more sizable for $\tan \beta = 1$. Also for the production of a heavy Higgs boson we see that the electroweak corrections are basically even in $\sin \alpha$ for large $\tan \beta$.

For the production of a heavy Higgs boson H_h we observe in Fig. 5 cusps for a heavy Higgs-boson mass of $M_{H_h} = 2M_{H_l}$. These cusps are threshold singularities which arise from the external heavy Higgs-boson wave function renormalization factor. Such threshold singularities of the processes considered here have been analyzed in detail in the SM in

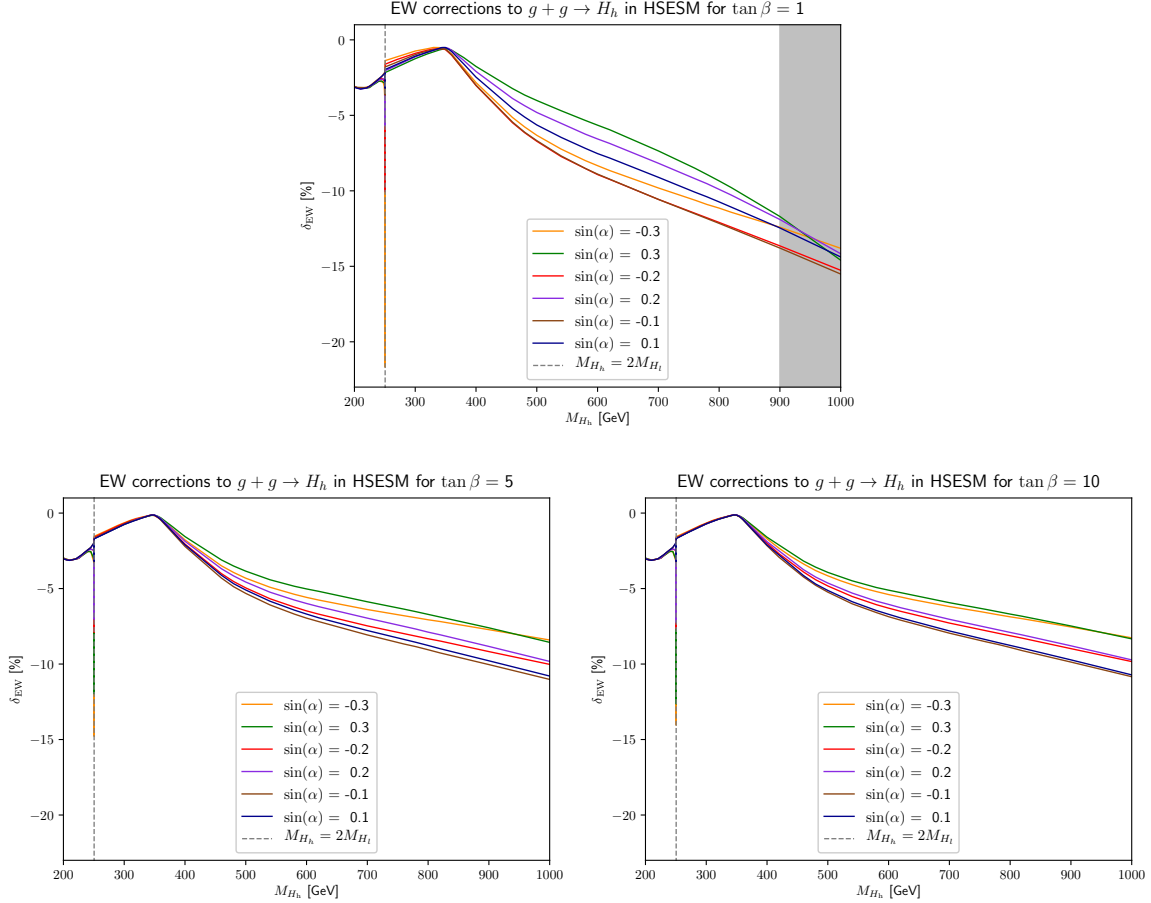


Figure 5: Relative NLO electroweak percentage corrections δ_{EW} in the OS scheme to the LO partonic cross section of the process $g + g \rightarrow H_h$ in the HSESM for $\tan \beta = 1, 5, 10$ with varying values of $\sin \alpha$.

Ref. [36]. Here, these singularities are regularized in the complex mass scheme by the complex light Higgs-boson mass. Since the total decay width of the light Higgs-boson is, however, very small, see Eq. (28), the cusps do not completely disappear and remain visible in the electroweak percentage corrections.

For the BPs of Tab. 1 we show the electroweak percentage corrections in Tab. 3 for the process $g + g \rightarrow H_h$. The mixing angle α has been renormalized in the OS scheme. The BPs follow the shape of the plots of Fig. 5. For Higgs-boson masses going from 200 GeV to 300 GeV the percentage correction increases, reaching a maximum close to zero for the benchmark point BHM300. For BPs with a larger value of the heavy Higgs-boson mass the electroweak percentage correction decreases. Comparing for a fixed value of the heavy Higgs-boson mass the BPs with suffix a (BHM400a \pm , BHM500a \pm , BHM700a \pm and BHM800a \pm) to those BPs with suffix b (BHM400b, BHM500b, BHM700b and BHM800b), respectively, we see that the electroweak percentage corrections for $g + g \rightarrow H_h$ are more sensitive to the sign of $\sin \alpha$ than to small changes in $\tan \beta$.

BP	δ_{EW}	BP	δ_{EW}	BP	δ_{EW}
BHM200–	–3.1	BHM400b	–1.7	BHM700a–	–7.6
BHM200+	–3.1	BHM500a–	–5.2	BHM700a+	–6.9
BHM300–	–0.7	BHM500a+	–4.2	BHM700b	–6.9
BHM300+	–1.1	BHM500b	–4.2	BHM800a–	–8.2
BHM400a–	–2.3	BHM600–	–6.7	BHM800a+	–7.9
BHM400a+	–1.7	BHM600+	–5.8	BHM800b	–7.9

Table 3: The electroweak percentage corrections δ_{EW} [%] in the OS scheme are shown for the benchmark points of Tab. 1.

The electroweak percentage corrections which we provide in Fig. 5 and Tab. 3 also apply to the partial decay width of the process $H_h \rightarrow g + g$ due to Eq. (19).

Now we want to compare the three renormalization schemes under consideration, i.e. the OS scheme, the $\bar{\Psi}\Psi$ scheme and the ZZ scheme as introduced in Section 3.3. In Fig. 6 we report the corrections for the light Higgs-boson production for $\sin \alpha = \pm 0.1$ and ± 0.3 . We consider only $\tan \beta = 1$ and 10, since the behaviour for $\tan \beta = 5$ is close to the one for $\tan \beta = 10$. For large values of $\tan \beta$ we show just the behaviour for negative $\sin \alpha$, since the corrections are essentially even in $\sin \alpha$ in this case.

The electroweak corrections remain stable (and close to the SM) for small values of $\sin \alpha$, however, it can be seen that the ZZ scheme is slightly shifted upwards from the SM line for the whole range of heavy Higgs-boson masses under consideration. This feature is even enhanced for $\sin \alpha = \pm 0.3$. In particular for $\sin \alpha = -0.3$ large differences between the ZZ scheme and the other two schemes exist and the ZZ scheme shows a large dependence on the heavy Higgs-boson mass M_{H_h} , which enhances the correction at large M_{H_h} values. For $\tan \beta = 1$, going from negative $\sin \alpha = -0.3$ to positive $\sin \alpha = +0.3$, the percentage correction of the $\bar{\Psi}\Psi$ scheme is shifted upwards by approximately the same amount as the OS scheme is shifted downwards. Fixing instead now $\sin \alpha = -0.3$ and going from $\tan \beta = 1$ to $\tan \beta = 10$ the $\bar{\Psi}\Psi$ scheme is shifted downwards stronger than the OS scheme. Since for large $\tan \beta$ the corrections are insensitive to the sign of $\sin \alpha$, the corrections for $\tan \beta = 10$ and $\sin \alpha = -0.3$ are comparable to the corrections for $\tan \beta = 10$ and $\sin \alpha = +0.3$. Thus the shift in the $\bar{\Psi}\Psi$ scheme is even larger when going from $\tan \beta = 1$ to $\tan \beta = 10$ for the positive value of $\sin \alpha = +0.3$. Hence the $\bar{\Psi}\Psi$ scheme displays a stronger dependence on $\tan \beta$ than the OS scheme. The difference in the three schemes is the renormalization of the mixing angle α as shown by the explicit expressions for the counterterm $\delta\alpha$ in Section 3.3. A peculiarity of the ZZ scheme is that its counterterm $\delta\alpha$ of Eq. (24) has an additional term, $c_\alpha s_\alpha (\delta_{H_l ZZ} - \delta_{H_h ZZ})$, which incorporates the information about the amplitudes of the processes $H_l \rightarrow Z + Z$ and $H_h \rightarrow Z + Z$. Such a term is absent in the $\bar{\Psi}\Psi$ and OS schemes of Eqs. (26) and (27), causing the overall shift of the percentage correction in the ZZ scheme compared to the other schemes as well as its stronger M_{H_h} dependence (for negative values of $\sin \alpha$). Furthermore, both the counterterm corresponding to the $\bar{\Psi}\Psi$ scheme and the ZZ scheme depend on all Higgs

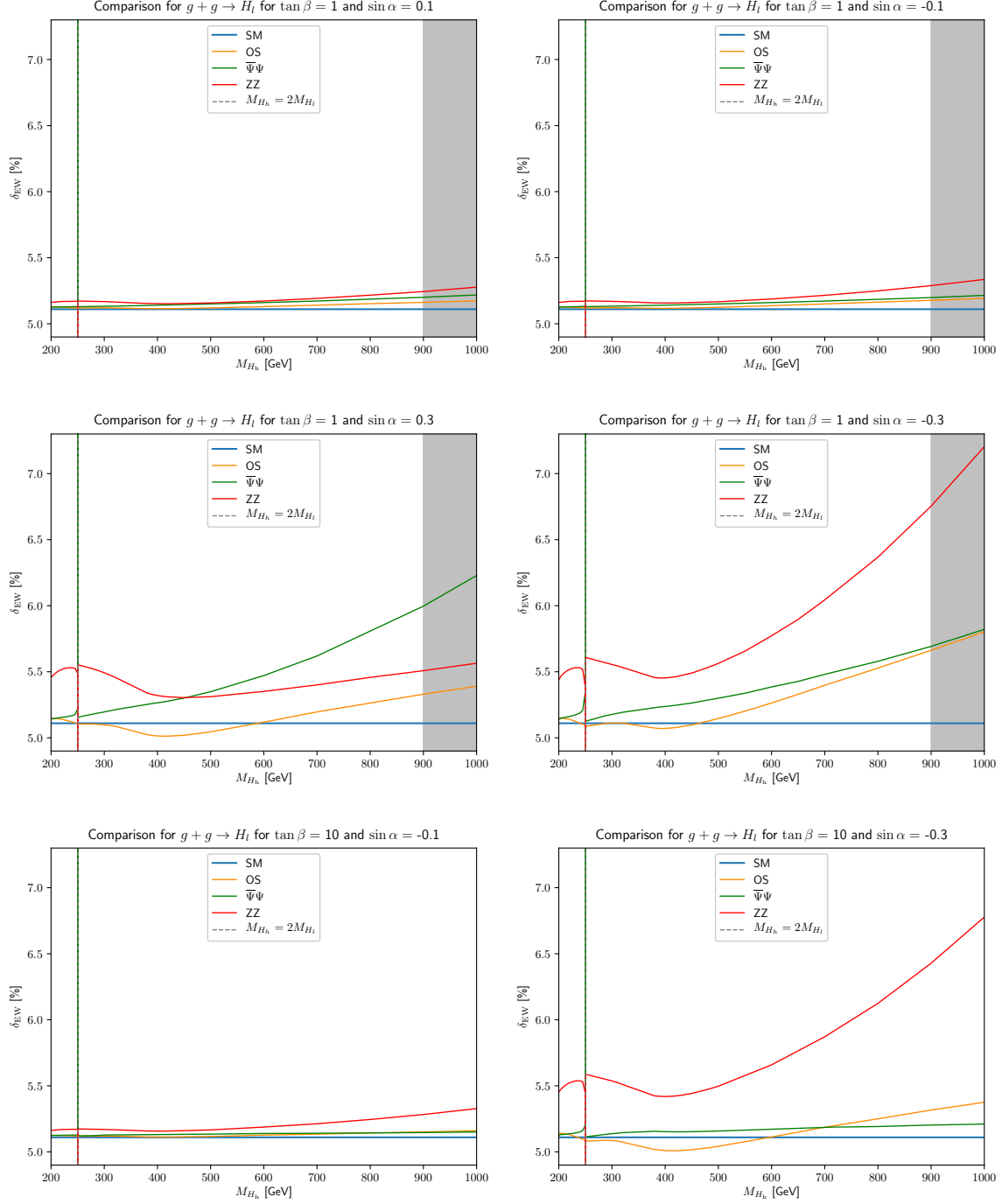


Figure 6: Comparison of the renormalization schemes for $g + g \rightarrow H_l$ in the HSESM for $\tan \beta = 1, 10$ with varying values of $\sin \alpha$. The SM limit is shown in blue.

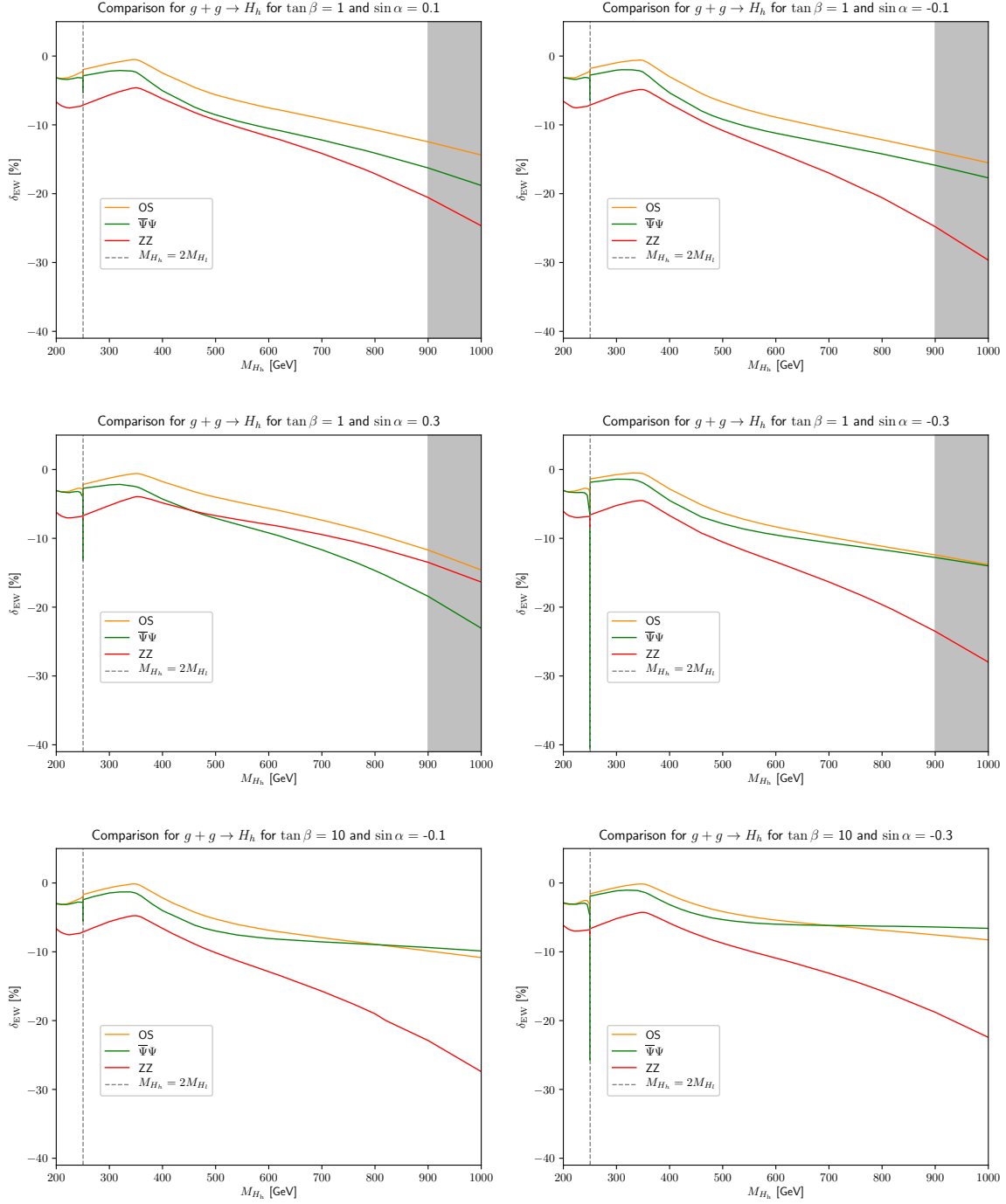


Figure 7: Comparison of the renormalization schemes for $g + g \rightarrow H_h$ in the HESM for $\tan\beta = 1, 10$ with varying values of $\sin\alpha$.

field strength renormalization factors of Eq. (23), whereas the counterterm corresponding to the OS scheme only depends on the off-diagonal ones. Since the $\tan\beta$ dependence originates from the trilinear Higgs couplings, the presence of the additional diagonal field strength renormalization factors in the $\overline{\Psi}\Psi$ scheme and the ZZ scheme introduces also an additional $\tan\beta$ dependence.

For the process of light Higgs-boson production there is no physical threshold singularity at $M_{H_h} = 2M_{H_l}$. As a result of this there are no cusps in Fig. 4 in the OS scheme, but only a small kink is visible for $M_{H_h} = 2M_{H_l}$. Analyzing Fig. 6 we observe for the ZZ and $\overline{\Psi}\Psi$ schemes that also for the process $g + g \rightarrow H_1$ threshold singularities appear for $M_{H_h} = 2M_{H_l}$. These threshold singularities are introduced artificially through the two process dependent renormalization schemes as already mentioned in Section 3.3. Both schemes rely on processes, where the decay of a heavy Higgs-boson enters, i.e. $H_h \rightarrow Z + Z$ for the ZZ scheme and $H_h \rightarrow \Psi + \overline{\Psi}$ for the $\overline{\Psi}\Psi$ scheme. In these two processes the heavy Higgs-boson wave function factor, which contains the threshold singularity, enters again. Thus these two schemes introduce the threshold singularities artificially into the process $g + g \rightarrow H_1$. Also for that reason we consider the result in the OS-scheme as our final result, which is free of this drawback.

The dependence on the renormalization scheme for the heavy Higgs-boson production in gluon fusion is shown in Fig. 7. The results in the ZZ scheme appear shifted compared to the OS scheme, being always at least 4% different. The reason for this shift is again the first term of Eq. (24) as already described in the discussion of the light Higgs-boson production in gluon fusion earlier in this section. For negative values of $\sin\alpha$ the ZZ scheme shows in addition a strong dependence on the heavy Higgs-boson mass, arriving at differences of the order of 15% for $M_{H_h} = 1000$ GeV between the ZZ scheme and the other schemes. Going for the fixed value of $\tan\beta = 1$ from negative $\sin\alpha = -0.3$ to positive $\sin\alpha = +0.3$, the percentage correction of the $\overline{\Psi}\Psi$ scheme is shifted downwards by approximately the same amount as the ZZ scheme is shifted upwards. For large values of $|\sin\alpha| = 0.3$ the $\overline{\Psi}\Psi$ scheme shows again a stronger dependence on $\tan\beta$ than the other schemes. In all three schemes the EW percentage corrections have a maximum between $M_{H_h} = 300$ GeV and $M_{H_h} = 400$ GeV, but the precise location and its shape are scheme dependent. In Fig. 7 one can see the threshold singularities for $M_{H_h} = 2M_{H_l}$, which are present in the plots for all schemes as expected. They are again regularized in the complex mass scheme by the complex light Higgs-boson mass, but remain as cusps since the width of the light Higgs boson is very small. The depth of the cusp caused by this threshold is strongly scheme dependent, with a deep cusp in the $\overline{\Psi}\Psi$ scheme and a hardly visible one in the ZZ scheme.

4.2 Higgs-boson decay into two photons in the HSESM

In this section we present results for the light and heavy Higgs-boson decay into two photons. Like in Section 4.1 for the Higgs-boson production in gluon fusion, we choose also here for the Higgs-boson decay into two photons the OS scheme as defined in Section 3.3 as reference renormalization scheme for the mixing angle α .

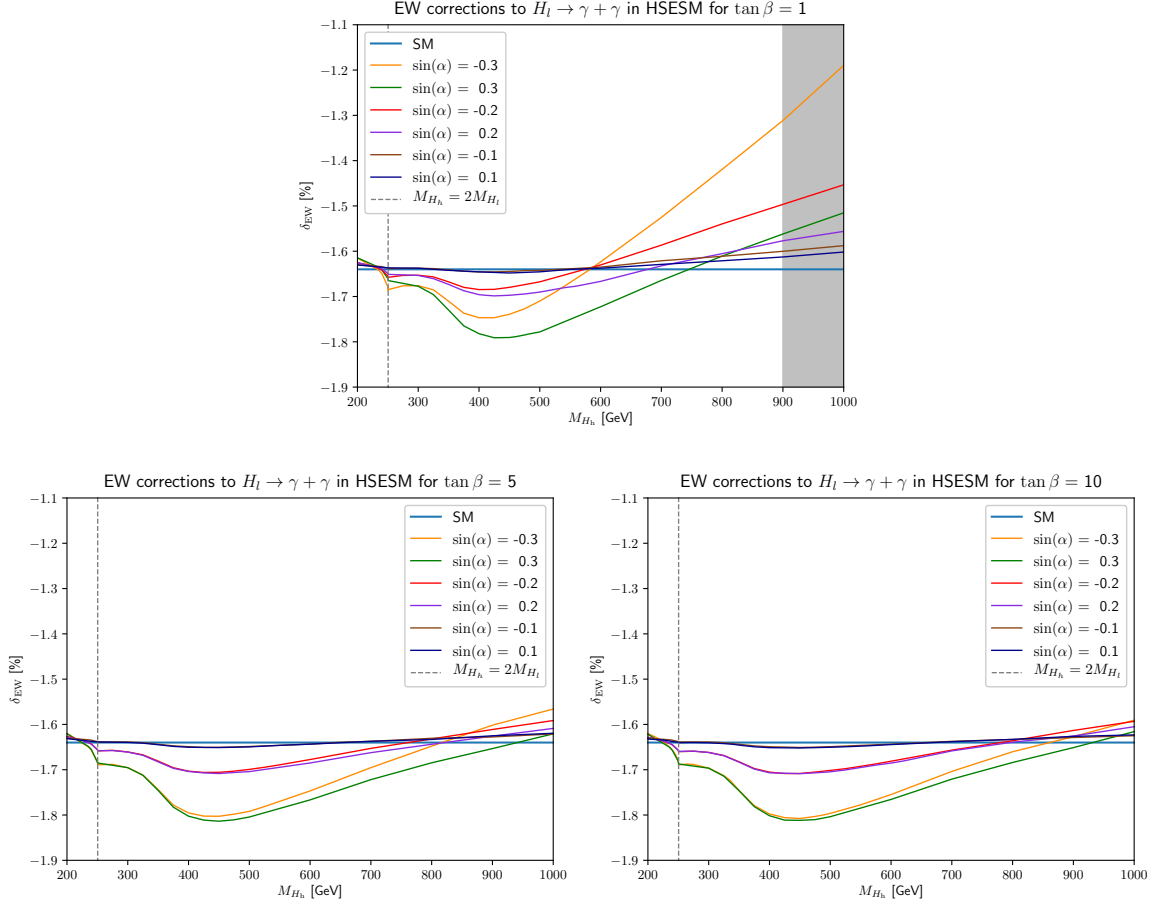


Figure 8: NLO electroweak percentage corrections δ_{EW} in the OS scheme relative to the LO partial decay width of the process $H_l \rightarrow \gamma + \gamma$ in the HSESM for $\tan \beta = 1, 5, 10$ with varying values of $\sin \alpha$. The SM limit is shown in blue.

In Fig. 8 we show the electroweak percentage corrections δ_{EW} defined in Eq. (21) as a function of the heavy Higgs-boson mass M_{H_h} for the decay of a light Higgs boson for 6 values of $\sin \alpha$. The three plots of Fig. 8, for the three values of $\tan \beta = 1, 5$ and 10 , show again the same numerical range for the percentage correction and the heavy Higgs-boson mass in order to allow to better compare the results for the three different values of $\tan \beta$. The SM result is again shown as the solid horizontal blue line in each plot. The electroweak corrections are negative and very close to the SM case. They range between about -1.8% to about -1.2% and are thus hardly to distinguish from the SM case. The largest deviations from the SM result can be observed again for high values of M_{H_h} , small values of $\tan \beta$ and large absolute values of $\sin \alpha$. Similarly to light Higgs-boson production in gluon fusion of Section 4.1 the electroweak percentage corrections δ_{EW} for the light Higgs-boson decay into two photons shows also here a minimum between around $M_{H_h} \approx 400 - 500$ GeV. Afterwards the percentage corrections grow again almost linearly. For the small value of $\tan \beta = 1$ in the first plot of Fig. 8 the different lines for the various

values of $\sin \alpha$ differ more from each other than for larger values of $\tan \beta = 5, 10$, where the dependence of the electroweak corrections on the sign of $\sin \alpha$ becomes again negligible due to the $\tan \beta$ -suppression already discussed in the previous Section 4.1. This can be seen best again in the last plot of Fig. 8 (for $\tan \beta = 10$), where the lines for $\pm \sin \alpha$ approach each other and almost coincide.

For the BPs of Tab. 1 we show the electroweak percentage corrections for the process $H_1 \rightarrow \gamma + \gamma$ in Tab. 4, where the mixing angle α has been renormalized in the OS scheme. The corrections are very close to the result of the SM and follow the shape of the plots in Fig. 8 with a slight minimum around $M_{H_h} \approx 400 - 500$ GeV.

BP	δ_{EW}	BP	δ_{EW}	BP	δ_{EW}
BHM200−	−1.6	BHM400b	−1.8	BHM700a−	−1.7
BHM200+	−1.6	BHM500a−	−1.7	BHM700a+	−1.7
BHM300−	−1.7	BHM500a+	−1.8	BHM700b	−1.7
BHM300+	−1.7	BHM500b	−1.8	BHM800a−	−1.6
BHM400a−	−1.7	BHM600−	−1.7	BHM800a+	−1.6
BHM400a+	−1.8	BHM600+	−1.7	BHM800b	−1.6

Table 4: The electroweak percentage corrections δ_{EW} [%] for the decay process $H_1 \rightarrow \gamma + \gamma$ are shown for the benchmark points of Tab. 1 for the mixing angle α in the OS scheme.

The electroweak percentage corrections for the heavy Higgs-boson decay into two photons in the HSESM are shown in Fig. 9 in three plots as a function of the heavy Higgs-boson mass M_{H_h} . The three plots are again for the three values of $\tan \beta = 1, 5, 10$ and show the six values of $\sin \alpha = \pm 0.1, \pm 0.2, \pm 0.3$. All three plots cover again the same range for the heavy Higgs-boson mass and the electroweak percentage correction, which allows to compare the three scenarios. While the electroweak percentage corrections for small heavy Higgs-boson masses around 200-300 GeV are only of the order of a few percent, they range from about -80% to about $+40\%$ for heavy Higgs-boson masses around 600 GeV and can thus become very large. Due to the wide range from large positive to large negative electroweak corrections, the different curves for the different values of $\sin \alpha$ are hard to distinguish.

The electroweak corrections have a maximum of 30%–42% for a heavy Higgs-boson mass between 570 GeV and 585 GeV, a turning point for a heavy Higgs-boson mass of $M_{H_h} \approx 630$ GeV and reach a minimum of -70% to -78% for a heavy Higgs-boson mass in the range of 675 GeV to 690 GeV. The exact size and location of the extrema depend on $\tan \beta$ and $\sin \alpha$. Again, for a small value of $\tan \beta = 1$ the curves for different values of $\sin \alpha$ are further apart than for large values of $\tan \beta = 5, 10$, where the curves with identical $|\sin \alpha|$ approach each other and essentially coincide for $\tan \beta = 10$ due to the $\tan \beta$ -suppression. For $\tan \beta = 1$ the maximum for $\sin \alpha = -0.3$ is located at $M_{H_h} = 585$ GeV with a value of around 42%, whereas the maximum for $\sin \alpha = +0.3$ is located at $M_{H_h} = 570$ GeV with a value of around 30%. The location and size of the minimum behave in a similar way with the minimum of -70% being located at

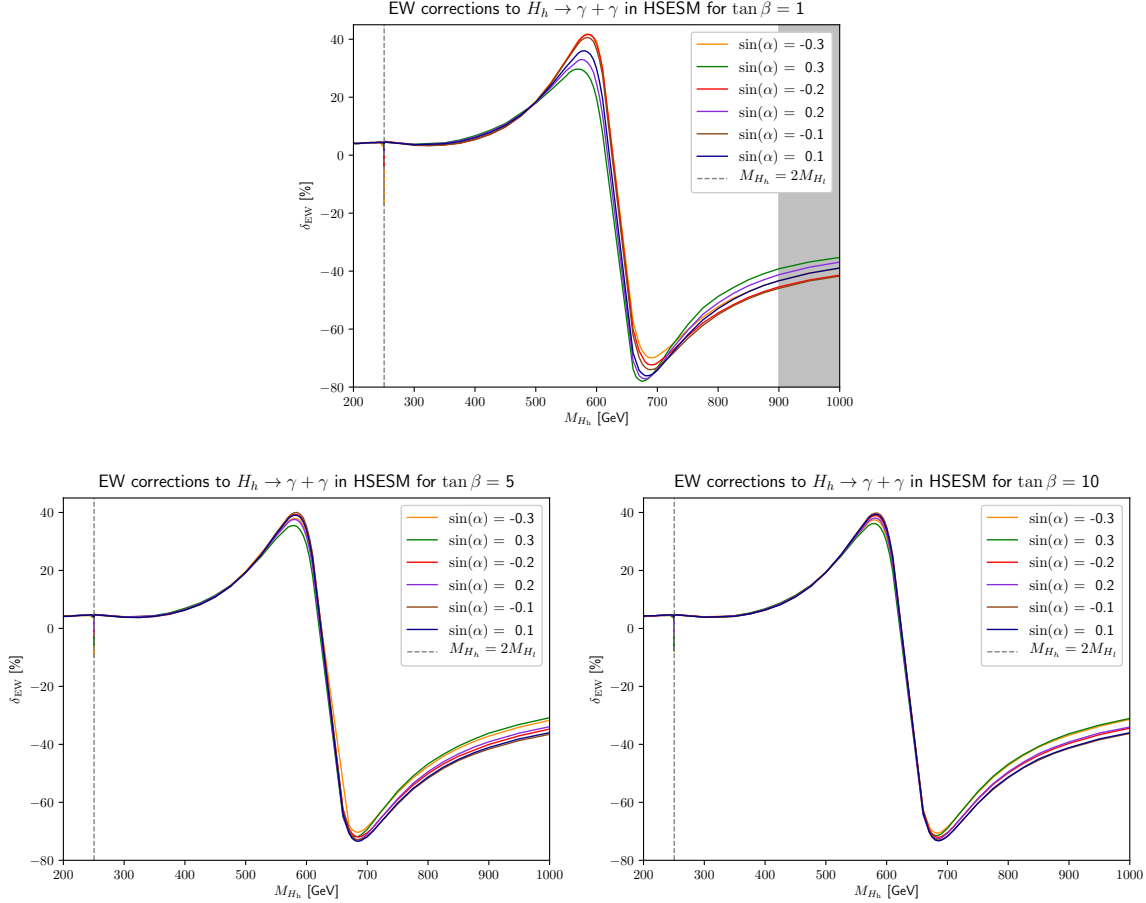


Figure 9: NLO electroweak percentage corrections δ_{EW} relative to the LO partial decay width of the process $H_h \rightarrow \gamma + \gamma$ in the HSESM for $\tan \beta = 1, 5, 10$ with varying values of $\sin \alpha$. The mixing angle α is renormalized in the OS scheme.

$M_{H_h} = 690$ GeV for $\tan \beta = 1$ and $\sin \alpha = -0.3$ and the minimum of -78% being located at $M_{H_h} = 675$ GeV for $\tan \beta = 1$ and $\sin \alpha = +0.3$. The reason for the fast change from large positive to large negative corrections within a few GeV of the heavy Higgs-boson mass can be understood when taking into account Fig.2(b), where the squared modulus of the LO amplitude $|A_{\gamma\gamma}^{\text{LO}}|^2$ is shown. There the squared modulus of the amplitude strongly decreases for Higgs-boson masses larger than about 300 GeV and reaches a minimum between 630-640 GeV, where the squared modulus becomes almost zero. After the minimum it increases only slightly (see inset of Fig.2(b)), but stays close to zero. The electroweak percentage corrections δ_{EW} of Fig. 9 being according to Eq. (21) an interference between the LO and NLO amplitude normalized to the squared modulus of the LO amplitude inherit this feature from the LO amplitude in the form of a large enhancement factor. In fact, the real and imaginary parts of the pure two-loop amplitude only change moderately for Higgs-boson masses between 600–700 GeV. However, the LO-NLO interference is such that it changes sign in this region. This change of sign paired

with the large enhancement leads to a very sharp drop.

We observe a cusp for a heavy Higgs-boson mass of $M_{H_h} = 2M_{H_1}$ in Fig. 9; this time also for a renormalization of the mixing angle α in the OS scheme. The cusp at the threshold of $M_{H_h} = 2M_{H_1}$ originates from the heavy Higgs-boson wave function factor. This threshold is here in this process $H_h \rightarrow \gamma + \gamma$ a real physical threshold and not introduced artificially due to the choice of the renormalization scheme, like for the processes $g+g \rightarrow H_1$ and $H_1 \rightarrow \gamma+\gamma$ in the ZZ or $\bar{\Psi}\Psi$ schemes. This threshold singularity is here again regularized by the complex mass of the light Higgs boson.

For the BPs of Tab. 1 we show the electroweak percentage corrections in Tab. 5 for the process $H_h \rightarrow \gamma + \gamma$. The mixing angle α is renormalized in the OS scheme. For smaller values of the heavy Higgs-boson mass between 200 to 400 GeV the electroweak corrections of the BPs are of moderate size and are of the order of a few percent. They coincide with what one expects from Fig. 9 in this mass range. Approaching heavy Higgs-boson masses of 500 to 600 GeV the electroweak corrections of the BPs are large and positive in accordance with Fig. 9. All BPs which only differ in the sign of $\sin \alpha$ are very close to each other, except for the benchmark point BHM600 \pm . The latter BP is close to the location where in Fig. 9 the percentage correction changes from large positive to large negative corrections and the curve has a steep slope. Thus the percentage correction vastly changes in a small window of a few GeV explaining the different percentage correction for BHM600 $-$ and BHM600 $+$. The large negative size of the electroweak corrections for the benchmark points BHM700 and BHM800 has the same reason as the large negative corrections in Fig. 9, i.e. the squared modulus of the LO amplitude becomes small. Studying the benchmark points BHM400a \pm , BHM400b, BHM500a \pm , BHM500b, BHM700a \pm , BHM700b, BHM800a \pm and BHM800b we see that the electroweak percentage corrections for $H_h \rightarrow \gamma + \gamma$ are more sensitive to the sign of $\sin \alpha$ than to small changes in $\tan \beta$ as was already the case for $g + g \rightarrow H_h$.

BP	δ_{EW}	BP	δ_{EW}	BP	δ_{EW}
BHM200 $-$	4.0	BHM400b	6.7	BHM700a $-$	-70.3
BHM200 $+$	4.0	BHM500a $-$	19.2	BHM700a $+$	-71.0
BHM300 $-$	3.8	BHM500a $+$	19.1	BHM700b	-71.0
BHM300 $+$	3.9	BHM500b	19.1	BHM800a $-$	-50.0
BHM400a $-$	6.0	BHM600 $-$	35.1	BHM800a $+$	-49.4
BHM400a $+$	6.7	BHM600 $+$	29.6	BHM800b	-49.4

Table 5: The electroweak percentage corrections δ_{EW} [%] for the decay process $H_h \rightarrow \gamma + \gamma$ are shown for a renormalization of the mixing angle α in the OS scheme.

Now we compare again the results for the electroweak percentage corrections in the three different renormalization schemes for the mixing angle α under consideration in this paper for the two decay processes $H_1 \rightarrow \gamma + \gamma$ and $H_h \rightarrow \gamma + \gamma$. The reasoning for the choices of $\sin \alpha$ and $\tan \beta$ in Fig. 10 and also in Fig. 11 is the same as the one described already in Section 4.1 for Figs. 8 and 9.

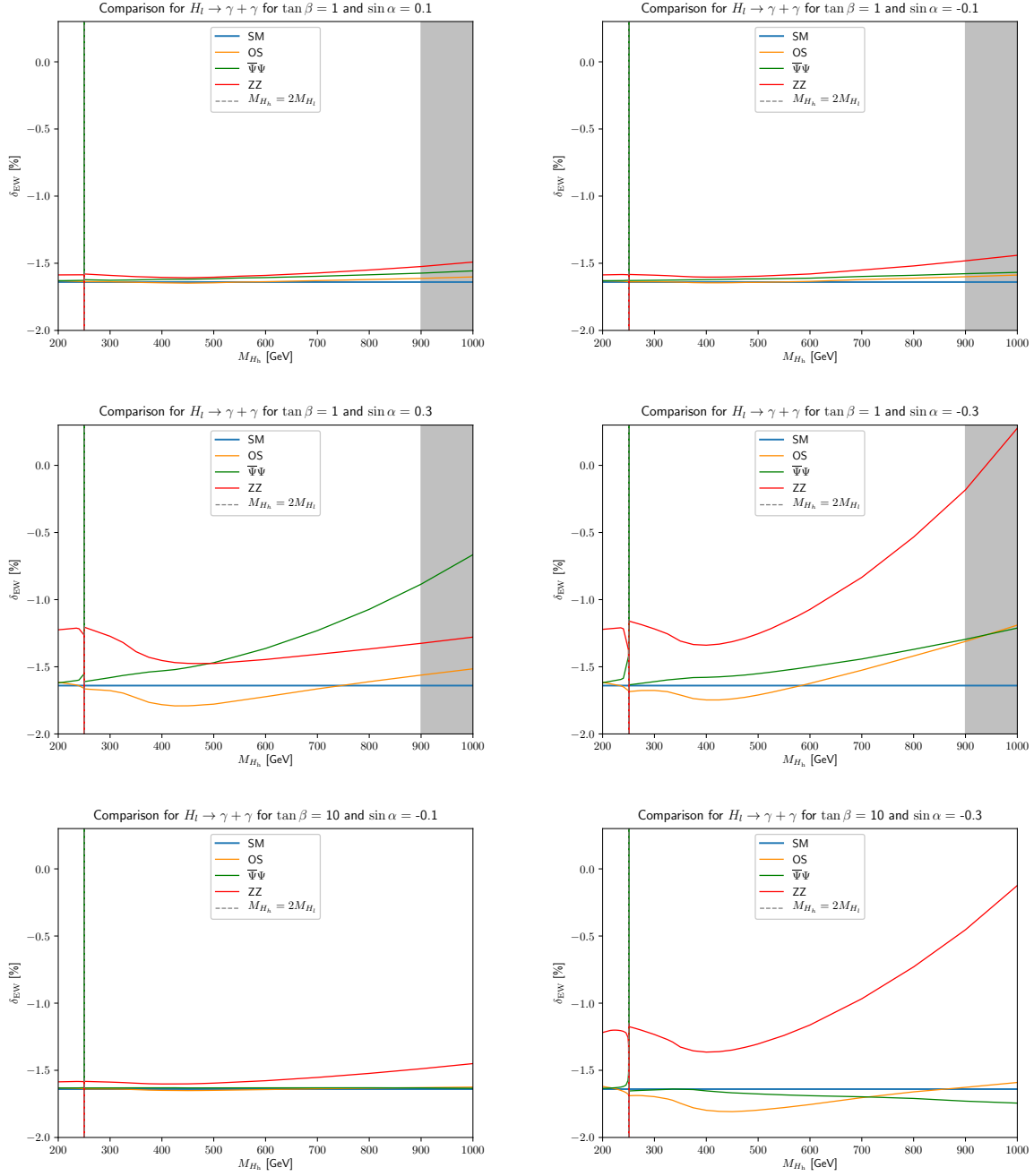


Figure 10: Comparison of the different renormalization schemes for the mixing angle α for the decay process $H_l \rightarrow \gamma + \gamma$ in the HSESM for $\tan \beta = 1, 10$ with varying values of $\sin \alpha$. The SM limit is shown by the blue line.

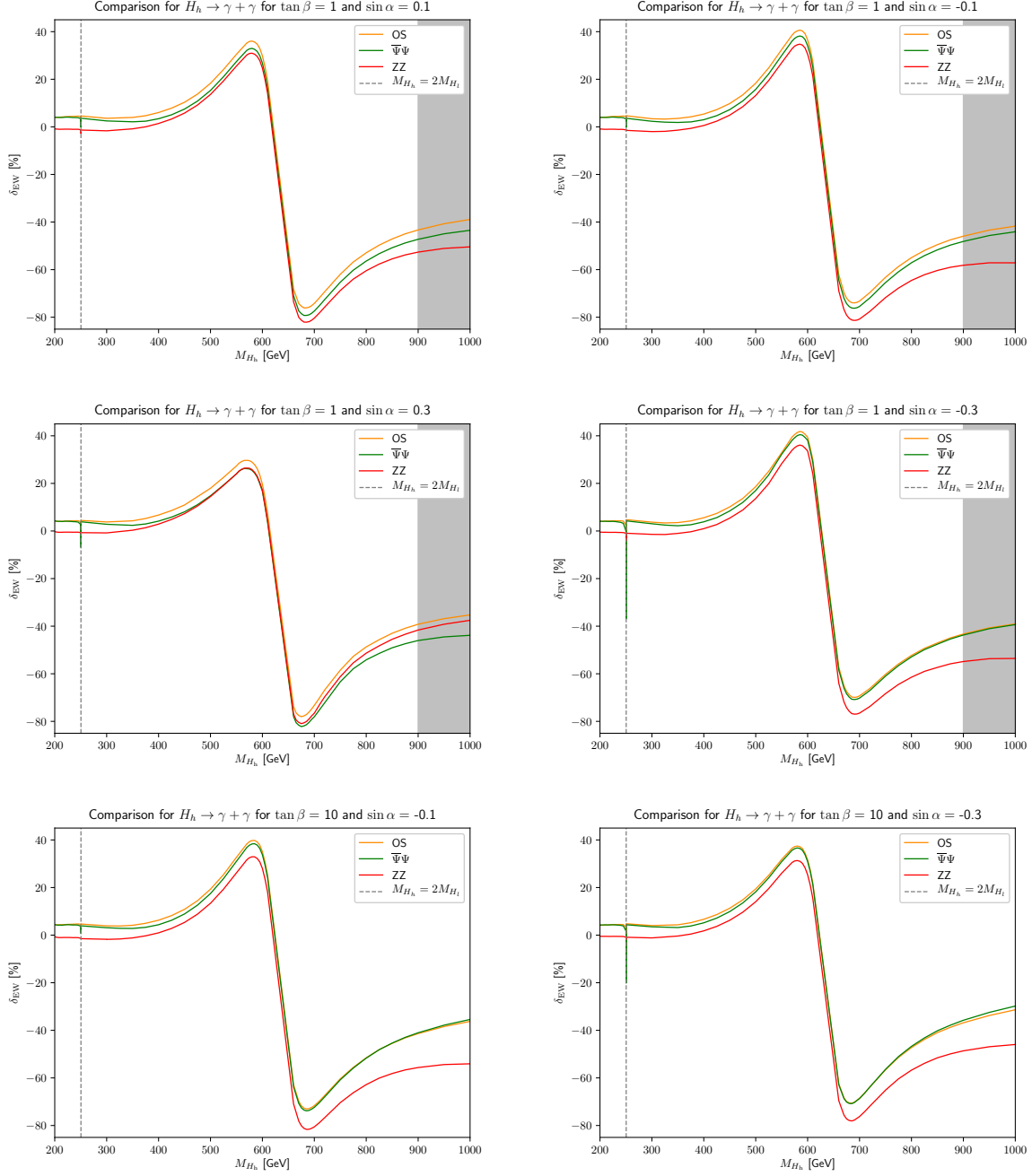


Figure 11: Comparison of the different renormalization schemes for the mixing angle α for the decay $H_h \rightarrow \gamma + \gamma$ in the HESM for $\tan\beta = 1, 10$ with varying values of $\sin\alpha$.

We start in Fig. 10 with the NLO electroweak percentage corrections as a function of the heavy Higgs-boson mass M_{H_h} for the process $H_1 \rightarrow \gamma + \gamma$. All six plots show again the same range for the electroweak percentage corrections and the heavy Higgs-boson mass in order to allow for an easy comparison of the different scenarios. The comparison plots show features similar to the case of $g + g \rightarrow H_1$. As before, the two process dependent ZZ - and $\bar{\Psi}\Psi$ -schemes contain the artificially introduced threshold singularities for $M_{H_h} = 2M_{H_1}$. For the values $\sin \alpha = \pm 0.1$ the three schemes are hardly distinguishable since we are close to the SM case. However, also for this process the ZZ scheme is shifted upwards from the SM for all values of $\tan \beta$ and $\sin \alpha$. Its sensitivity to the sign of $\sin \alpha$ is demonstrated by comparing the plots with $\tan \beta = 1$ and $\sin \alpha = \pm 0.3$. In particular, for $\sin \alpha = -0.3$ we observe again a strong dependence of the ZZ scheme on M_{H_h} . In addition, the $\bar{\Psi}\Psi$ scheme shows the strongest dependence on $\tan \beta$. Despite the fact that the differences for $\sin \alpha = -0.3$ look large we want to note that the percentage corrections only cover a small range of about 1.5%, so that also the differences between the schemes are at most of the same size.

In Fig. 11 we compare likewise the three different renormalization schemes for the NLO electroweak percentage corrections of the decay $H_h \rightarrow \gamma + \gamma$. All three schemes show the threshold singularity at $M_{H_h} = 2M_{H_1}$, with a strong dependence of the size of the cusp on the scheme. As it was the case for heavy Higgs-boson production in gluon fusion the lowest value of the electroweak percentage corrections at this threshold is obtained in the $\bar{\Psi}\Psi$ scheme, whereas barely any cusp is visible in the ZZ scheme. Another similarity to the process $g + g \rightarrow H_h$ is the fact that the ZZ scheme is shifted downwards compared to the OS scheme. In contrast to all other processes, the ZZ scheme here does not show the strongest M_{H_h} dependence for negative values of $\sin \alpha$ and large heavy Higgs-boson mass M_{H_h} . Indeed in this mass region the dependence on M_{H_h} is milder in this case than for positive $\sin \alpha$. For $\sin \alpha = -0.3$ large differences between the ZZ scheme and the other two schemes exist and the ZZ scheme shows a weak dependence on the heavy Higgs-boson mass M_{H_h} . The $\bar{\Psi}\Psi$ scheme again shows the strongest dependence on $\tan \beta$ for $\sin \alpha = +0.3$ when going from $\tan \beta = 1$ to $\tan \beta = 10$. Since for large $\tan \beta$ the corrections are insensitive to the sign of $\sin \alpha$, the corrections for $\tan \beta = 10$ and $\sin \alpha = +0.3$ are comparable to the corrections for $\tan \beta = 10$ and $\sin \alpha = -0.3$.

Among the considered schemes the OS-scheme is the one which does not introduce artificial threshold singularities for $M_{H_h} = 2M_{H_1}$ for the light Higgs-boson production and decay processes studied in this paper. The ZZ scheme can in addition lead to large corrections due to the existence of finite process dependent contributions (first term of Eq. (24)). As a result of this we consider the results in the OS scheme as our final results.

5 Summary and conclusion

We have computed the two-loop electroweak corrections for four loop-induced processes in the real Higgs-Singlet Extensions of the Standard Model (HSESM). For the Higgs-boson production we considered the light and heavy Higgs-boson production in gluon fusion. For the Higgs-boson decay we considered the light and heavy Higgs-boson decays into two photons. The HSESM has three additional new input parameters compared to the Standard Model (SM) which are the new heavy Higgs-boson mass, the mixing angle α and the ratio of the two vacuum expectation values $\tan\beta$. The latter needs not to be renormalized for the above processes, while for the mixing angle α we consider three renormalization schemes from literature among which we choose the on-shell scheme for our final results.

The few new parameters of the HSESM allow us to provide the electroweak percentage corrections to these processes for scans over a wide range of the new input parameters. In addition we also provide the results for benchmark scenarios which have been collected by the Higgs cross section working group.

The electroweak corrections for light Higgs-boson production through gluon fusion and for the decay into two photons are in both cases very close to the SM. The electroweak corrections for heavy Higgs-boson production are negative and can reach up to about -10% in the on-shell scheme for large heavy Higgs-boson masses. The heavy Higgs-boson decay into two photons shows an interesting feature. The electroweak percentage corrections change here from large positive corrections to large negative corrections within about ± 50 GeV for heavy Higgs-boson masses of around 630 GeV. This feature is inherited from the leading-order amplitude which becomes very small in this region explaining thus the large size of the electroweak corrections.

Acknowledgments

We would like to thank Ansgar Denner, Stefan Dittmaier, Jean-Nicolas Lang and Giampiero Passarino for valuable discussions. The work of B.S. and C.S. was supported by the Deutsche Forschungsgemeinschaft (DFG) under contract STU 615/2-1.

References

- [1] ATLAS Collaboration, G. Aad *et al.*, *Phys. Lett. B* **716** (2012) 1–29, 1207.7214; CMS Collaboration, S. Chatrchyan *et al.*, *Phys. Lett. B* **716** (2012) 30–61, 1207.7235.
- [2] V. Silveira and A. Zee, *Phys. Lett. B* **161** (1985) 136–140; J. McDonald, *Phys. Rev. D* **50** (1994) 3637–3649, hep-ph/0702143.
- [3] T. Binoth and J. J. van der Bij, *Z. Phys. C* **75** (1997) 17–25, hep-ph/9608245; R. M. Schabinger and J. D. Wells, *Phys. Rev. D* **72** (2005) 093007, hep-ph/0509209; B. Patt and F. Wilczek, hep-ph/0605188; M. Bowen, Y. Cui, and J. D. Wells, *JHEP* **03** (2007) 036, hep-ph/0701035; V. Barger, P. Langacker, M. McCaskey, M. J. Ramsey-Musolf, and G. Shaughnessy, *Phys. Rev. D* **77** (2008) 035005, 0706.4311.
- [4] Particle Data Group Collaboration, P. Zyla *et al.*, *PTEP* **2020** (2020), no. 8, 083C01.
- [5] ATLAS Collaboration, G. Aad *et al.*, *JHEP* **11** (2015) 206, 1509.00672; CMS Collaboration, V. Khachatryan *et al.*, *JHEP* **10** (2015) 144, 1504.00936.
- [6] ATLAS Collaboration, G. Aad *et al.*, *Phys. Lett. B* **800** (2020) 135103, 1906.02025.
- [7] A. Denner, J.-N. Lang, and S. Uccirati, *JHEP* **07** (2017) 087, 1705.06053.
- [8] L. Altenkamp, M. Boggia, and S. Dittmaier, *JHEP* **04** (2018) 062, 1801.07291.
- [9] A. Denner, S. Dittmaier, and J.-N. Lang, *JHEP* **11** (2018) 104, 1808.03466.
- [10] N. Kauer, A. Lind, P. Maierhöfer, and W. Song, *JHEP* **07** (2019) 108, 1905.03296.
- [11] F. Bojarski, G. Chalons, D. Lopez-Val, and T. Robens, *JHEP* **02** (2016) 147, 1511.08120.
- [12] M. Boggia, R. Gomez-Ambrosio, and G. Passarino, *JHEP* **05** (2016) 162, 1603.03660.
- [13] T. Robens, in *55th Rencontres de Moriond on QCD and High Energy Interactions*. 2021. 2105.07719; A. Ilnicka, T. Robens, and T. Stefaniak, *Mod. Phys. Lett. A* **33** (2018), no. 10n11, 1830007, 1803.03594; R. Costa, M. Mühlleitner, M. O. P. Sampaio, and R. Santos, *JHEP* **06** (2016) 034, 1512.05355; G. M. Pruna and T. Robens, *Phys. Rev. D* **88** (2013), no. 11, 115012, 1303.1150.
- [14] T. Robens and T. Stefaniak, *Eur. Phys. J. C* **76** (2016), no. 5, 268, 1601.07880.

- [15] LHC Higgs Cross Section Working Group Collaboration, D. de Florian *et al.*, [1610.07922](#).
- [16] G. Passarino, C. Sturm, and S. Uccirati, *Phys. Lett. B* **655** (2007) 298–306, [0707.1401](#).
- [17] S. Actis, G. Passarino, C. Sturm, and S. Uccirati, *Phys. Lett. B* **670** (2008) 12–17, [0809.1301](#).
- [18] S. Actis, G. Passarino, C. Sturm, and S. Uccirati, *Nucl. Phys. B* **811** (2009) 182–273, [0809.3667](#).
- [19] G. Passarino, C. Sturm, and S. Uccirati, *Phys. Lett. B* **706** (2011) 195–199, [1108.2025](#).
- [20] A. Denner, S. Dittmaier, A. Mück, G. Passarino, M. Spira, C. Sturm, S. Uccirati, and M. M. Weber, *Eur. Phys. J. C* **72** (2012) 1992, [1111.6395](#).
- [21] A. Denner, L. Jenniches, J.-N. Lang, and C. Sturm, *JHEP* **09** (2016) 115, [1607.07352](#); L. Jenniches, C. Sturm, and S. Uccirati, *PoS RADCOR2017* (2018) 065, [doi:10.22323/1.290.0065](#).
- [22] L. Jenniches, C. Sturm, and S. Uccirati, *JHEP* **09** (2018) 017, [1805.05869](#).
- [23] K. G. Chetyrkin, J. H. Kühn, and M. Steinhauser, *Comput. Phys. Commun.* **133** (2000) 43–65, [hep-ph/0004189](#).
- [24] A. Alloul, N. D. Christensen, C. Degrande, C. Duhr, and B. Fuks, *Comput. Phys. Commun.* **185** (2014) 2250–2300, [1310.1921](#); N. D. Christensen and C. Duhr, *Comput. Phys. Commun.* **180** (2009) 1614–1641, [0806.4194](#).
- [25] P. Nogueira, *J. Comput. Phys.* **105** (1993) 279–289.
- [26] J. A. M. Vermaseren, [math-ph/0010025](#); B. Ruijl, T. Ueda, and J. Vermaseren, [1707.06453](#).
- [27] G. Passarino and S. Uccirati, *Nucl. Phys. B* **629** (May, 2002) 97–187, [hep-ph/0112004](#); A. Ferroglia, M. Passera, G. Passarino, and S. Uccirati, *Nucl. Phys. B* **680** (Mar, 2004) 199–270, [hep-ph/0311186](#); G. Passarino and S. Uccirati, *Nucl. Phys. B* **747** (Jul, 2006) 113–189, [hep-ph/0603121](#).
- [28] N. M. Korobov, *The approximate calculation of multiple integrals using number theoretic methods Dokl. Acad. Nauk SSSR* **115** (1957) 1062–1065; N. M. Korobov, *Number-theoretic methods in approximate analysis, Fizmatgiz, Moscow* (1963); H. Conroy and B. L. Bruner, *The Journal of Chemical Physics* **47** (1967), no. 3, 5307–5318.

- [29] A. Denner, S. Dittmaier, M. Roth, and D. Wackeroth, *Nucl. Phys. B* **560** (1999) 33–65, [hep-ph/9904472](#); A. Denner, S. Dittmaier, M. Roth, and L. H. Wieders, *Nucl. Phys. B* **724** (2005) 247–294, [hep-ph/0505042](#); A. Denner and S. Dittmaier, *Nucl. Phys. B Proc. Suppl.* **160** (2006) 22–26, [hep-ph/0605312](#).
- [30] J. Fleischer and F. Jegerlehner, *Phys. Rev. D* **23** (1981) 2001–2026.
- [31] S. Actis, A. Ferroglia, M. Passera, and G. Passarino, *Nucl. Phys. B* **777** (2007) 1–34, [hep-ph/0612122](#).
- [32] S. Dittmaier and H. Rzehak, *JHEP* **05** (2022) 125, [2203.07236](#); S. Dittmaier and H. Rzehak, *JHEP* **08** (2022) 245, [2206.01479](#).
- [33] S. Kanemura, Y. Okada, E. Senaha, and C. P. Yuan, *Phys. Rev. D* **70** (2004) 115002, [hep-ph/0408364](#).
- [34] A. Denner, J.-N. Lang, and S. Uccirati, *Comput. Phys. Commun.* **224** (2018) 346–361, [1711.07388](#).
- [35] B. Summ, C. Sturm, and S. Uccirati, *Electroweak corrections to $gg \rightarrow H$ and $H \rightarrow \gamma\gamma$ in the singlet extended Standard Model*, *Conference presentation in 29th International Workshop on Deep-Inelastic Scattering and Related Subjects* (2022) [doi:10.5281/zenodo.7254998](#).
- [36] S. Actis, G. Passarino, C. Sturm, and S. Uccirati, *Phys. Lett. B* **669** (2008) 62–68, [0809.1302](#).